Plexin-A4 Mediates Cytotoxic T-cell Trafficking and Exclusion in Cancer

Ward Celus[1,2], Ana I. Oliveira[1,2,3,4], Silvia Rivis[1,2], Heleen H. Van Acker[1,2], Ewout Landeloos[5,6], Jens Serneels[1,2], Sarah Trusso Cafarello[1,2], Yannick Van Herck[7], Roberta Mastrantonio[8], Arnaud Köhler[9,10], Abhishek D. Garg[11], Véronique Flamand[9,10], Luca Tamagnone[8,12], Jean-Christophe Marine[5,6], Mario Di Matteo[1,2], Bruno M. Costa[3,4], Oliver Bechter[7], and Massimiliano Mazzone[1,2]

ABSTRACT

Cytotoxic T cell (CTL) infiltration of the tumor carries the potential to limit cancer progression, but their exclusion by the immunosuppressive tumor microenvironment hampers the efficiency of immunotherapy. Here, we show that expression of the axon guidance molecule Plexin-A4 (*Plxna4*) in CTLs, especially in effector/memory $CD8^+$ T cells, is induced upon T-cell activation, sustained in the circulation, but reduced when entering the tumor bed. Therefore, we deleted *Plxna4* and observed that *Plxna4*-deficient CTLs acquired improved homing capacity to the lymph nodes and to the tumor, as well as increased proliferation, both achieved through enhanced Rac1 activation. Mice with stromal or hematopoietic *Plxna4* deletion exhibited enhanced CTL infiltration and impaired tumor growth. In a melanoma model, adoptive transfer of CTLs lacking *Plxna4* prolonged survival and improved therapeutic outcome, which was even stronger when combined with anti–programmed cell death protein 1 (PD-1) treatment. *PLXNA4* abundance in circulating CTLs was augmented in melanoma patients versus healthy volunteers but decreased after the first cycle of anti–PD-1, alone or in combination with anti–cytotoxic T-Lymphocyte Associated Protein 4 (CTLA-4), in those patients showing complete or partial response to the treatment. Altogether, our data suggest that Plxna4 acts as a "checkpoint," negatively regulating CTL migration and proliferation through cell-autonomous mechanisms independent of the interaction with host-derived Plxna4 ligands, semaphorins. These findings pave the way toward Plxna4-centric immunotherapies and propose Plxna4 detection in circulating CTLs as a potential way to monitor the response to immune checkpoint blockade in patients with metastatic melanoma.

Introduction

Immunotherapy has emerged as a promising treatment for patients with advanced cancer. Immune system–based cancer therapies offer a durable clinical benefit because they can potentiate a self-propagating and adaptable response once the immune system is activated (1). However, only a fraction of patients responds to such treatment (2). Most of the immunotherapy-resistant tumors are "cold," entailing a severely impaired presence and activation status of effector T cells within the tumor microenvironment (TME; ref. 3). Thus, understanding the mechanisms underlying T-cell exclusion could translate into a broader and more durable response to this therapeutic option.

Cytotoxic $CD8^+$ T lymphocytes (CTL) are one of the most powerful antitumor cells in the TME and their infiltration in tumors correlates with good prognosis in several tumor types (4). Immune checkpoint inhibitors (ICI) take advantage of these cells and their killing capacity, but these require both the presence and physical contact between antitumor T cells and cancer cells (1). Given the lack of preexisting CTLs in T-cell "cold" tumors, it is very unlikely that the use of currently approved ICIs will lead to robust antitumoral T-cell responses in these tumor types (5). Hence, priming of the tumor via a combination of different therapies might be used to recruit a higher number of CTLs into these tumors.

Plexins are large transmembrane glycoproteins that, in most cases, function as the receptors for semaphorins (6). In the nervous system, these proteins play a bifunctional role, having the capacity to exert both repulsive and attractive effects in neuronal wiring during development (7). Their ability to modulate the immune response in both physiological and pathological conditions (8) and their role as "cell positioning cues" within the TME have also been explored (9).

[1]Laboratory of Tumor Inflammation and Angiogenesis, Center for Cancer Biology, VIB, Leuven, Belgium. [2]Laboratory of Tumor Inflammation and Angiogenesis, Department of Oncology, KU Leuven, Leuven, Belgium. [3]Life and Health Sciences Research Institute (ICVS), School of Medicine, University of Minho, Braga, Portugal. [4]ICVS/3B's - PT Government Associate Laboratory, Braga/Guimarães, University of Minho, Braga, Portugal. [5]Laboratory for Molecular Cancer Biology, Center for Cancer Biology, VIB, Leuven, Belgium. [6]Laboratory for Molecular Cancer Biology, Department of Oncology, KU Leuven, Leuven, Belgium. [7]Department of General Medical Oncology, University Hospitals Leuven, Department of Oncology, KU Leuven, Leuven, Belgium. [8]Department of Life Sciences and Public Health, Università Cattolica del Sacro Cuore, Rome, Italy. [9]Institute for Medical Immunology, ULB-Center for Research in Immunology, Gosselies, Belgium. [10]Institute for Medical Immunology, Université Libre de Bruxelles, Gosselies, Belgium. [11]Laboratory of Cell Stress & Immunity, Department of Cellular and Molecular Medicine, KU Leuven, Leuven, Belgium. [12]Fondazione Policlinico Universitario Agostino Gemelli IRCCS, Rome, Italy.

W. Celus and A.I. Oliveira contributed equally to this article.

Corresponding Author: Massimiliano Mazzone, VIB Center for Cancer Biology, Department of Oncology, University of Leuven, Campus Gasthuisberg, Herestraat 49, Box 912, Leuven B-3000, Belgium. Phone: 321-637-3213; Fax: 321-637-2585; E-mail: massimiliano.mazzone@kuleuven.be

Cancer Immunol Res 2022;10:126–41

doi: 10.1158/2326-6066.CIR-21-0061

Targeting plexin signals (or semaphorins) is therefore a promising therapeutic strategy to restore antitumor immunity.

Plexin-A4 (*Plxna4*) is a member of class A plexins (10), which interacts with Sema6A and Sema6B (11). When in association with neuropilin-1 (NRP1), it can also function as a coreceptor for Sema3A (12). In the central nervous system, Plxna4 mediates axon repulsion by the direct binding to Sema6A and Sema6B (13, 14). In the immune system, Plxna4 has been implicated in macrophage Toll-like receptor (TLR)-mediated signaling and cytokine production in sepsis (15), anti-inflammatory polarization in colitis (16), and entry into hypoxic niches in cancer (17). In T cells, Plxna4 negatively regulates T-cell–mediated immune responses, with *Plxna4*-deficient mice showing exacerbated disease in a mouse model of experimental autoimmune encephalomyelitis (EAE; ref. 18). On the basis of these findings, we defined the function of PlxnA4 in the control of the immune response in the context of cancer.

Materials and Methods

Animals

Plxna4 knockout (KO) mice on a C57BL/6 background were obtained from Dr. Castellani (Institut NeuroMyoGène, Université de Lyon, Lyon, France). C57BL/6 mice were purchased from Charles River. OT-I mice were purchased from Taconic. *Sema6a* KO mice on a C57BL/6 background were obtained from Prof. Dr. Pasterkamp (Dept. of Translational Neuroscience, University Medical Center Utrecht, The Netherlands). All mice used were between 6 and 12 weeks old, without specific gender selection. In all experiments, littermate controls were used. Euthanasia was performed by cervical dislocation. Housing conditions and all experimental animal procedures were approved by the Animal Ethics Committee of the KU Leuven.

Bone marrow transplantation

Six-week-old C56BL/6 recipient mice were lethally irradiated with a dose of 9.5 Gy using the Small Animal Radiation Research Platform (SARRP, XSTRAHL). Femur and tibia bones were collected from donor mice of the appropriate genotype. In a sterile culture hood, bone marrow (BM) cells were obtained by flushing the bones with a syringe filled with Roswell Park Memorial Institute (RPMI) 1640 medium (Gibco, Thermo Fisher Scientific, 21875034) supplemented with 10% heat-inactivated FBS (Biowest, S1810). The cells were subsequently filtered using a 40-μm pore–sized mesh and centrifuged for 5 minutes at 200 × *g*. BM cells were counted and 1×10^7 cells were injected intravenously (i.v.) via tail vein in the irradiated recipient mice. Tumor experiments were initiated 6 to 8 weeks after BM reconstitution. Red and white blood cell count was determined using a hemocytometer on peripheral blood, collected in heparin with capillary pipettes by retro-orbital bleeding.

Cell lines

Murine Lewis lung carcinoma cells (LLC) and B16F10 melanoma cells were obtained from the ATCC. E0771 medullary breast adenocarcinoma cells were obtained from CH3Biosystems. All cells were cultured in Dulbecco's Modified Eagle Medium (DMEM; Gibco, Thermo Fisher Scientific, 41965039) supplemented with 10% heat-inactivated FBS, 2 mmol/L glutamine (Gibco, Thermo Fisher Scientific, 25030024), 100 U/mL penicillin, and 100 μg/mL streptomycin (Gibco, Thermo Fisher Scientific, 15140122) at 37°C in a humidified atmosphere containing 5% CO_2. For the overexpression of ovalbumin (OVA), the following plasmid was used: pCDH_CMV7-OVA-EFI-G418. LLC and B16F10 cancer cells were transduced with concentrated lentiviral vectors and further selected with G418 antibiotics (1 mg/mL, Invivogen, ant-gn) to generate a homogenous population of OVA-overexpressing cancer cells (LLC-OVA and B16F10-OVA). Overexpression of the OVA protein was confirmed by Western blot analysis. All cell lines were tested for *Mycoplasma* and passaged in the laboratory for no longer than 6 months after receipt.

Tumor models

Adherent growing murine cells, 1×10^6 LLC and 5×10^5 B16F10, were injected subcutaneously (s.c.) for LLC and orthotopically for B16F10 at the right side of the mouse in PBS (Gibco, Thermo Fisher Scientific, 14190094). Alternatively, 5×10^5 E0771 medullary breast adenocarcinoma cells were injected orthotopically in the mammary fat pad of the second nipple on the right side in a volume of 50 μL PBS. Tumor volumes were measured three times a week with a caliper and calculated using the formula: $V = \pi \times d^2 \times D/6$, where d is the minor tumor axis and D is the major tumor axis. At the end stage, tumors were weighed and collected for immunofluorescence and/or flow cytometric analyses. For survival analysis, a tumor volume of 1,800 mm^3 was used as the humane endpoint.

Histology and immunostaining

Tumors and lymph nodes (LN) were collected and fixed in 4% formaldehyde (37% stock, VWR, ACRO119690250) diluted in PBS overnight at 4°C, dehydrated and embedded in paraffin. Serial sections were cut at 7-μm thickness with an HM 355S automatic microtome (Thermo Fisher Scientific). Paraffin slides were first rehydrated to further proceed with antigen retrieval in Target Retrieval Solution, Citrate pH 6.1 (DAKO, Agilent, S1699). If necessary, 0.3% hydrogen peroxide (Stock 30%, Millipore, 1072090250) was added to methanol (VWR, 20848.320), to block endogenous peroxidases. The sections were blocked with the appropriate serum (DAKO, Agilent), matching the species of the secondary antibody, and incubated overnight at room temperature with the following antibodies: rat anti-CD8α (Thermo Fisher Scientific, 4SM15, 1:100), rat anti-CD4 (Thermo Fisher Scientific, 4SM95, 1:100), rat anti-F4/80 (AbD Serotec, MCA497, 1:100), rabbit anti-FITC (AbD Serotec, 4510–7604, 1:200), rat anti-CD31 (BD Pharmingen, 550274, 1:50), rat anti-CD34 (BD Pharmingen, 553731, 1:100), rabbit anti-NG2 (Millipore, AB5320, 1:200), and rat anti-PNAd (BioLegend, MECA-79, 1:100). Appropriate secondary antibodies raised against the species of the primary antibody were used: Alexa 488 (Molecular Probes, A21208, 1:200), 647 (Molecular Probes, A31573, 1:100) or 568-conjugated secondary antibodies (Molecular Probes, A11077, 1:200), biotin-labeled antibodies (Jackson Immunoresearch, 711–065–152 and 712–065–153, 1:300), and, when necessary, TSA Plus Cyanine 3 and Cyanine 5 System amplification (Perkin Elmer, Life Sciences, NEL744001KT and NEL745001KT, 1:50) were performed according to the manufacturer's instructions. Hoechst-33342 solution (Thermo Fisher Scientific, H3570, 1:1,000) was used to visualize nuclei. Mounting of slides was done with ProLong Gold mounting medium without DAPI (Invitrogen, P36930). Imaging and microscopic analysis was performed with an Olympus BX41 microscope and CellSense imaging software.

Tumor hypoxia assessment and tumor perfusion

Tumor hypoxia was detected 1 hour after intraperitoneal (i.p.) injection of 60 mg/kg pimonidazole hydrochloride (Hypoxyprobe kit, Chemicon, HP3–100Kit) in LLC tumor–bearing mice. Tumors were harvested and fixed in 4% formaldehyde overnight. To detect the formation of pimonidazole adducts, 7-μm thick sections were immunostained with rabbit anti-hypoxyprobe monoclonal (Hypoxyprobe

Kit, Chemicon, HP3–100 Kit, 1:100) following the manufacturer's instructions. Perfused tumor vessels were counted on tumor sections from mice injected i.v. with 0.05 mg FITC-conjugated lectin (Lycopersicon esculentum; Vector Laboratories, B-1175–1).

Flow cytometry

Mice were sacrificed by cervical dislocation, and tumors, livers, blood, LNs (inguinal and axillary LNs) or the tumor-draining LN (tdLN; the closest LN draining the tumor bed) were collected. Tumors were minced in α-minimum essential medium (MEM) (Lonza, BE12–169F), containing 50 μmol/L β-mercaptoethanol (Gibco, Thermo Fisher Scientific, 21985023), 5 U/mL Deoxyribonuclease I 0.85 mg/mL (Roche, 10104159001), Collagenase V (Sigma-Aldrich, C9263–1G), 1.25 mg/mL Collagenase D (Roche, 11 088 882 001), and 1 mg/mL Dispase (Gibco, Thermo Fisher Scientific, 17105–041), and incubated in the same solution for 30 minutes at 37°C. Livers were processed in RPMI 1640 medium, supplemented with 10 U/mL Deoxyribonuclease I (Roche, 10104159001) and 120 U/ml Collagenase III (Worthington Biochemical, LS004182), using the gentleMACS Dissociator (Miltenyi Biotec). The digested tissues were filtered using a 70-μm pore–sized mesh and cells were centrifuged for 5 minutes at 300 × *g*. Blood samples were collected in heparin with capillary pipettes by retro-orbital bleeding. Red blood cell lysis was performed by using a homemade red blood cell lysis buffer (150 mmol/L NH_4Cl, 0.1 mmol/L EDTA, 10 mmol/L $KHCO_3$, pH 7.4). LNs were processed on a 40-μm pore cell strainer in sterile PBS and cells were centrifuged for 10 minutes at 300 × *g*. Red blood cell lysis was performed by using Hybri-Max (Sigma-Aldrich, R7757). Single cells were resuspended in FACS buffer (PBS containing 2% FBS and 2 mmol/L EDTA) and incubated for 15 minutes with Mouse BD Fc Block purified anti-mouse CD16/CD32 (BD Pharmingen, 553142). Extracellular staining was performed for 30 minutes at 4°C. When necessary, permeabilization was performed using the eBioscience Foxp3/Transcription Factor Fixation/Permeabilization Kit (Thermo Fisher Scientific, 00–5521–00) according to the manufacturer's instructions and cells were incubated overnight at 4°C with the intracellular antibodies. All antibodies used are described in Supplementary Table S1. Cells were subsequently washed and resuspended in FACS buffer before flow cytometric analysis by a FACS Canto II, Fortessa X-20, or flow sorting by a FACS Aria III, Aria Fusion (BD Biosciences). Data were analyzed by FlowJo (TreeStar, Version 10.7). Fluorescence Minus One (FMO) controls were utilized to ensure proper gating of positive populations.

Mouse T-cell isolation and activation

Naïve mouse T cells were isolated from the spleen, inguinal, and axillary LNs. In brief, tissues were processed on a 40-μm pore cell strainer in sterile PBS and cells were centrifuged for 10 minutes at 300 × *g*. Red blood cell lysis was performed using Hybri-Max. Total splenocytes were cultured in T-cell medium [RPMI 1640 medium supplemented with 10% heat-inactivated FBS, 100 U/mL penicillin and 100 μg/mL streptomycin, 1% MEM non-essential amino acids (NEAA, Gibco, Thermo Fisher Scientific, 11140035), 25 μmol/L β-mercaptoethanol, and 1 mmol/L sodium pyruvate (Gibco, Thermo Fisher Scientific, 11360070)] at 37°C in a humidified atmosphere containing 5% CO_2.

According to the experimental requirements, T cells were activated for 3 days by adding mouse anti-CD3/CD28–coated Dynabeads (Thermo Fisher Scientific, 11453D) at a 1:1 bead-to-cell ratio. At day 3 of activation, the beads were magnetically removed and activated T cells were further expanded for a maximum of 3 additional days in the presence of 10 ng/mL recombinant murine IL2 (mIL2, PeproTech, 212–12). $CD8^+$ T cells were isolated by using MagniSort Mouse $CD8^+$ T Cell Negative Selection Kit (eBioscience, Thermo Fisher Scientific, 8804–6822–74) according to the manufacturer's instructions. $CD4^+$ T cells were isolated by using MACS Mouse $CD4^+$ T Cell Isolation Kit (Miltenyi Biotec, 130–104–454) according to the manufacturer's instructions. According to the experimental requirements, activated T cells (at day 3 of stimulation) were treated for 48 hours with 15 μg/mL anti–programmed cell death protein 1 (PD-1; RMP1–14, BioLegend) or the appropriate isotype control. FOXO inhibition in activated T cells at day 3 of stimulation was performed by 48 hours of treatment with 80 μmol/L carbenoxolone (CBX, Sigma-Aldrich, C4790) or the DMSO vehicle control (dimethyl sulfoxide, Sigma, D2438).

Human T-cell isolation and activation

Buffy coat samples from healthy donors were obtained from the Red Cross-Flanders. Human $CD4^+$ and $CD8^+$ T cells were directly isolated by using the StraightFrom Buffy Coat CD4 and CD8 MicroBead Kit (Miltenyi Biotec, 130–114–980 and 130–114–978, respectively) according to the manufacturer's instructions. Red blood cell lysis was performed using Hybri-Max. T cells were activated in T-cell medium for 3 days by adding human anti-CD3/CD28–coated Dynabeads (Thermo Fisher Scientific, 11132D) at a 1:1 bead-to-cell ratio. At day 3 of activation, the beads were magnetically removed and activated T cells were further expanded for a maximum of 7 additional days in the presence of 10 ng/mL recombinant human IL2 (hIL2, PeproTech, 200–02). According to the experimental requirements, activated T cells (at day 7 of stimulation) were treated for 48 hours with 15 μg/mL anti–PD-1 (J116, BioXCell) or the appropriate isotype control.

Cytospin staining

$CD8^+$ T cells and peripheral blood leukocytes were seeded onto glass slides by cytospin centrifugation and fixed in 4% formaldehyde for 10 minutes, followed by incubation with 0.2% Triton-X (VWR, 1.086.031.000) diluted in PBS for 15 minutes. To reduce the immune background, sections were blocked with 10% donkey serum (Sigma, D9663) in PBS for 1 hour, followed by blocking with FAB fragment anti-mouse IgG (Jackson Immunoresearch, 715–007–003, 1:10) for 1 hour. Samples were then probed overnight with mouse anti-Plexin-A4 (Plxna4; R&D Systems, 707201, 1:500) and incubated with Donkey Alexa 568–conjugated secondary antibodies (Molecular Probes, A10037, 1:100) for 45 minutes. Nuclei were counterstained with Hoechst-33342 and mounting of the slides was performed with ProLong Gold mounting medium without DAPI. All steps were performed at room temperature. Microscopy was conducted with an Olympus BX41 microscope and cellSens imaging software.

Quantitative RT-PCR

RNA was extracted from T cells using the TRIzol Reagent (Life Technologies, 15596018) according to the manufacturer's instructions. Reverse transcription to cDNA was performed with the SuperScript III First Strand cDNA Synthesis Kit (Life Technologies, 18080051) according to the manufacturer's instructions. Premade assays were purchased from Integrated DNA Technologies. The cDNA, primer/probe mix, and TaqMan Fast Universal PCR Master Mix were prepared according to the manufacturer's instructions (Applied Biosystems, 4352042). Samples were loaded into an optical 96-well Fast Thermal Cycling Plate (Applied Biosystems) and qRT-PCR was performed using a QuantStudio 12K Flex Real-Time PCR System (Applied Biosystems). Samples were run in technical

duplicates. Data was normalized to housekeeping gene expression (*Hprt* for mouse and *TBP* for human genes). The commercially available probes (Integrated DNA technologies) used are listed in Supplementary Table S2.

Lymphocytic choriomeningitis virus expressing OVA model

Wild-type (WT) mice were preconditioned by i.v. injection of 1×10^4 naïve OT-I T cells. Twenty-four hours later, the mice were vaccinated i.p. with 10^5 plaque-forming units (PFU) of a recombinant lymphocytic choriomeningitis virus expressing OVA (LCMV-OVA; a kind gift from Prof. Dr. Daniel Pinschewer, University of Basel, Basel, Switzerland), as described in Flatz and colleagues (19). After 7 days of LCMV-OVA infection, OT-I T cells were FACS sorted from the blood.

T-cell proliferation assay

To monitor cell proliferation, activated T cells were labeled with 3.5 μmol/L Violet Cell Tracer (Thermo Fisher Scientific, C34557) at 37°C for 20 minutes. The cells were subsequently washed with FACS buffer and cultured according to the experimental requirements. Absolute numbers of T cells in culture were counted by flow cytometry using Precision Count Beads (BioLegend, 424902). According to the experimental requirements, activated T cells (at day 3 of stimulation) were treated with 100 μmol/L Rac1 inhibitor NSC23766 (Selleckchem, S8031) or the DMSO vehicle control.

Annexin V/propidium iodide apoptosis assay

Activated $CD8^+$ T cells were collected, washed, and resuspended in 100 μL Annexin V Binding Buffer (BioLegend, 422201) containing 4 μL of Annexin V (BioLegend, 640941) and 0.1 μL propidium iodide solution (1 mg/mL stock, Sigma Aldrich, P4864). After 15 minutes of incubation at room temperature, samples were analyzed by flow cytometry.

Transwell migration assay

Migration of T cells was assessed by using Transwell permeable supports with 5-μm polycarbonate membrane (Costar, 3387). To determine cell migration in response to soluble factors, the bottom chamber was loaded with 0.1% FBS, 200 ng/mL CCL21 (PeproTech, 250–13), 200 ng/mL CCL19 (PeproTech, 250–27B), 150 ng/mL CXCL9 (PeproTech 250–18), or 50 ng/mL CXCL10 (PeproTech, 250–16) in T-cell medium. T cells were incubated for 2 (naïve) or 3 hours (activated) at 37°C and migrated cells in the bottom chamber were collected and counted by flow cytometry using Precision Count Beads. According to the experimental requirements, activated T cells were pretreated for 1 hour with 10 μg/mL anti-CCR7 (R&D Systems, 4B12), 250 μg/mL anti-CXCR3 (BioLegend, CXCR3–173), 100 μmol/L Rac1 inhibitor NSC23766, or the appropriate isotype, or vehicle control.

LN homing assay

Naïve $CD8^+$ T cells were isolated from WT and *Plxna4* KO mice and labeled with either 3.5 μmol/L Violet Cell Tracer or 1 μmol/L carboxyfluorescein diacetate succinimidyl ester (CFSE) Cell Tracer (Thermo Fisher Scientific, C34554). For CFSE labeling, cells were stained in PBS for 8 minutes at room temperature with gentle agitation. To label cells with Violet Cell Tracer, the staining was conducted for 20 minutes at 37°C with gentle agitation. Afterwards, a brief wash with complete RPMI medium was performed to quench any remaining dye. Healthy WT mice were injected i.v. with a 1:1 mixture between $1–2 \times 10^6$ labeled WT and *Plxna4* KO T cells. After 2 hours, LNs of the recipient mice were harvested and analyzed by IHC and/or flow cytometry. To exclude probe-specific cell toxicity, the fluorescent cell tracers were switched accordingly, showing identical experimental results.

Tumor homing assay

OT-I T cells were isolated from transgenic WT and *Plxna4* KO OT-I mice, generated by the intercross of *Plxna4* heterozygous mice with OT-I–positive mice. These mice have a monoclonal population of naïve T-cell receptor (TCR) transgenic $CD8^+$ T cells (OT-I T cells) that recognize the immunodominant cytosolic chicken OVA "SIINFEKL" peptide. For activation of OT-I T cells, total splenocytes from OT-I mice were isolated and cultured for 3 days in T-cell medium with 1 μg/mL SIINFEKL peptide (IBA - LifeSciences, 6–7015–901) and 10 ng/mL mIL2. At day 3 of activation, OT-I T cells were further expanded for a maximum of 3 additional days in the presence of 10 ng/mL mIL2.

For the tumor homing assay, activated WT and *Plxna4* KO OT-I T cells were labeled with either 3.5 μmol/L Violet Cell Tracer or 1 μmol/L CFSE and injected i.v. with a 1:1 mixture between $2–3 \times 10^6$ WT and *Plxna4* KO OT-I T cells into WT recipient mice with established B16F10-OVA or LLC-OVA tumors. The tumors of recipient mice were harvested 24 and 48 hours after T-cell transfer and analyzed by flow cytometry.

Liver homing assay

WT mice received a plasmid DNA by hydrodynamic injection (HDI). Each mouse was injected rapidly (<8 seconds) in the tail vein with 40 μg of pcDNA3 empty vector (EV) or pcDNA3-OVA (OVA) diluted in PBS in an injection volume of 10% of the body weight. Four days after HDI, activated WT and *Plxna4* KO OT-I T cells were labeled with either 3.5 μmol/L Violet Cell Tracer or 1 μmol/L CFSE and injected i.v. with a 1:1 mixture between $2–3 \times 10^6$ WT and KO OT-I T cells into mice. Twenty-four hours after T-cell transfer, blood and livers were harvested and analyzed by flow cytometry.

Plasmids and lentiviral vectors

In the overexpression experiments, the following plasmids were used: pCDH-CMV-Sema3a-DYK-EF1-Puro (*Sema3a* OE), pCDH-CMV-Sema6a-DYK-EF1-Puro (*Sema6a* OE), pCDH-CMV-Sema6b-DYK-EF1-Puro (*Sema6b* OE), and pCDH-CMV-MCS-EF1-Puro (EV). B16F10-OVA cancer cells were transduced with concentrated lentiviral vectors and further selected with puromycin antibiotics (1 μg/mL, Sigma, P9620) to allow the generation of a homogenous population of overexpressed (and empty vector control) cancer cells.

GTPase pull-down assay

Rac1 and Rap1 activation were measured by using a Rac1 or Rap1 Activation Assay Kit (Thermo Fisher Scientific, 16118 and 16120, respectively) according to the manufacturer's instructions. Briefly, cell lysis was performed by incubating activated T cells (at day 5 of stimulation) with the lysis buffer for 5 minutes on ice. The lysates were centrifuged for 15 minutes at 16,000 × *g* and subsequently incubated with the glutathione *S*-transferase (GST)-fused with: (i) p21-binding domain of Pak1 (GST-Pak1-PBD, 20 μg) or (ii) RalGDS-binding domain of Rap1 (GST-RalGDS-RBD, 20 μg), bound to glutathione resin at 4°C for 60 minutes with gentle rocking. After being washed three times with lysis buffer, the samples were eluted in 2× SDS reducing sample buffer and analyzed for bound Rac1 (GTP-Rac1) or Rap1 (GTP-Rap1) by Western blot analysis.

Western blotting

Protein extraction of liver samples was performed by using a homemade RIPA lysis buffer (50 mmol/L Tris HCl pH 8, 150 mmol/L NaCl, 1% Triton X-100, 0.5% sodium deoxycholate, 0.1% SDS) supplemented with Complete Protease Inhibitor Cocktail (Roche, 11697498001) and PhosSTOP Phosphatase Inhibitor (Roche, 04906837001). Lysates were incubated on ice for 30 minutes before centrifuging for 15 minutes at 4°C to remove cellular debris. Protein concentration of cell extracts was determined by using Pierce bicinchoninic acid (BCA) reagent (Thermo Fisher Scientific, 23227) according to the manufacturer's instructions. Protein samples were denaturated by adding a homemade 6X loading buffer (β-mercaptoethanol 0.6 mol/L; SDS 8%; Tris-HCl 0.25 mol/L pH 6,8; glycerol 40%; bromophenol blue 0.2%), incubated at 95°C for 5 minutes. Samples containing equivalent amounts of protein were subjected to 12% SDS-PAGE. Proteins were transferred onto a nitrocellulose membrane using the Trans-Blot Turbo Transfer System (Bio-Rad) according to manufacturer's instructions. The membranes were blocked for nonspecific binding in 5% nonfat dry milk (Cell Signaling Technology, 9999S) in homemade Tris-buffered saline-Tween 0.1% (50 mmol/L Tris HCl pH 7.6, 150 mmol/L NaCl, 0.1% Tween; TBS-T) for 1 hour at room temperature and incubated with primary antibody overnight at 4°C. The following antibodies were used: mouse anti-Rac1 (Thermo Fisher Scientific, 16118, 1:1,000), rabbit anti-Rap1 (Thermo Fisher Scientific, 16120, 1:1,000), mouse anti-Vinculin (Sigma-Aldrich, V9131, 1:200), and mouse anti-OVA (Abcam, ab17293, 1:500). After incubation with the primary antibodies, the membranes were washed for 15 minutes in TBS-T and incubated with the appropriate secondary antibody (1:5,000 in 5% nonfat dry milk in TBS-T) for 1 hour at room temperature. The following secondary antibodies were used: goat anti-mouse and goat anti-rabbit IgG-HRP (Santa Cruz Biotechnology, sc-2005 and sc-2004, respectively). The signal was visualized with Enhanced Chemiluminescent Reagents (ECL; Invitrogen, WP20005) or SuperSignal West Femto Chemiluminescent Substrate (Thermo Fisher Scientific, 34094) with a digital imager (ImageQuant LAS 4000, GE Health Care Life Science Technologies). The results of the GTPase pull-down assay were normalized against the corresponding band of the total proteins.

Adoptive T-cell transfer

Adoptive T-cell transfer (ACT) experiments were performed with either naïve or activated OT-I T cells. WT recipient mice carrying subcutaneous LLC-OVA or orthotopic B16F10-OVA tumors (average tumor size of 30–50 mm^3) were injected i.v. with either PBS, 1–3 $\times$ 10^6 WT or the same number of *Plxna4* KO OT-I T cells. Starting from the day of ACT, recipient mice were injected daily i.p. with 5 μg/mouse of recombinant human IL2 in a volume of 200 μL of PBS for 4 consecutive days. Recipient mice were additionally treated i.p. three times per week with 10 mg/kg anti–PD-1 (RMP1–14, BioLegend) or the appropriate isotype control, starting from an average tumor size of 200 mm^3. The tumors were measured every day and were weighted and collected at the end stage for flow cytometric analysis.

Human samples

Blood samples were freshly collected from patients with metastatic melanoma before and 3 weeks after the first cycle of ICI therapy (anti–PD-1 alone or in combination with anti–CTLA-4). Response assessment of patients with melanoma with stage III and IV nonresectable disease was performed as per response evaluation criteria in solid tumors (RECIST v1.1; ref. 20). Patients with complete or partial responses were categorized as responders, while nonresponders only achieved stable or progressive disease as their best overall response. Patients with resectable stage III disease all underwent complete LN dissection, which coincided with the "on-treatment" sampling time point. Pathologic response was assessed on the resection specimen. Patients with a complete response were categorized as responders, while patients without pathologic complete response were categorized as nonresponders. All relevant clinicopathologic information of the human subjects is provided in Supplementary Table S3. Inclusion and exclusion criteria for the study can be found in Supplementary Table S4. The research using human samples was conducted according to institutional and European Union ethical standards, and all subjects ensured written informed consent to participate in this study.

In brief, peripheral blood mononuclear cells from patients and healthy volunteers were immediately isolated by density gradient centrifugation using Lymphoprep (Stemcell, 07811). $CD4^+$ and $CD8^+$ T cells were negatively selected using MojoSort Human CD4 and CD8 T Cell Isolation Kit (Miltenyi Biotec, 480010 and 480129, respectively) according to manufacturer's instructions. For the expression analysis of circulating monocytes, cDNA samples from patients with different tumor types and age-matched healthy controls (Supplementary Table S5) were provided by the "Monomark" clinical study (21).

Statistical analysis

Data entry and all analyses were performed in a blinded fashion. All statistical analyses were performed using GraphPad Prism Software (Version 9.2). Pairwise comparisons on two experimental conditions were performed using an unpaired Student *t* test or a paired *t* test for competition assays. Grouped data were assessed by two-way ANOVA with Bonferroni multiple comparison correction. Survival curves were compared with the log-rank (Mantel–Cox) test. Statistical details of the experiments can be found in the figure legends. Detection of mathematical outliers was performed using the Grubbs test in GraphPad. Sample sizes for all experiments were chosen based on previous experiences. All graphs show mean values ± SEM.

Results

Genetic knockout of *Plxna4* in the stroma inhibits tumor progression and increases CTL infiltration

To study the role of Plxna4 in the TME, we took advantage of *Plxna4* KO mice (Supplementary Fig. S1A; ref. 22). Compared with WT controls, *Plxna4* KO mice were phenotypically identical and had similar blood counts (Supplementary Table S6). By implanting LLC cancer cells s.c., we observed a significantly slower tumor growth in *Plxna4* KO versus WT mice (**Fig. 1A** and **B**). Because previous experiments with human umbilical vein endothelial cells (HUVEC) have shown the involvement of *Plxna4* in basic fibroblast growth factor (bFGF)-induced angiogenic signaling (23), we analyzed tumor blood vessel parameters in WT and *Plxna4* KO mice. Tumor vessel density, perfusion, and pericyte coverage were comparable between WT and *Plxna4* KO mice (Supplementary Fig. S1B–S1D), resulting in no differences in tumor hypoxic areas (Supplementary Fig. S1E). *Plxna4* was also reported to be part of the signaling complex involved in the positioning of tumor-associated macrophages (TAM) inside hypoxic niches (17). However, we could not observe any difference in either TAM infiltration (Supplementary Fig. S1F) or localization within hypoxic regions (Supplementary Fig. S1G and S1H). In addition, gene expression markers typically used to characterize classically (M1-like) and alternatively activated (M2-like) macrophages were unaltered in

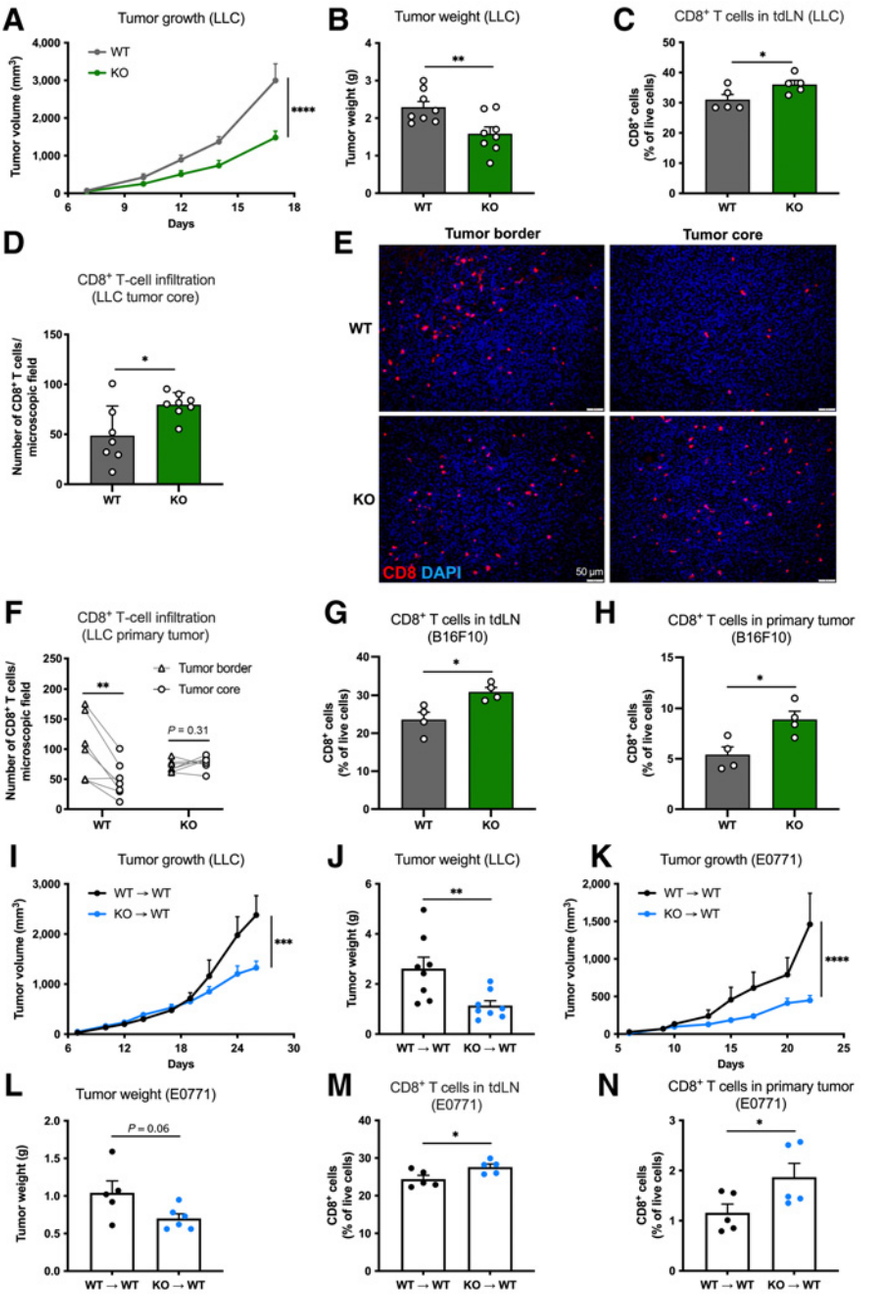

Figure 1.

Genetic knockout of *Plxna4* in the stroma or in the hematopoietic lineage abates tumor progression and increases CTL infiltration. Subcutaneous LLC tumor growth (**A**) and weight (**B**) in WT and *Plxna4* KO mice. **C,** Flow cytometric analysis of CTLs in the tdLNs from WT and *Plxna4* KO mice bearing subcutaneous LLC tumors. Histologic quantification of CTLs in the inner tumor bed (**D**), representative micrographs (scale bar, 50 μm; **E**), and paired analysis of the inner (core) and outer (border) tumor areas of LLC tumor sections obtained from WT and *Plxna4* KO tumor-bearing mice (**F**). Flow cytometric analysis of CTLs in the tdLNs (**G**) and orthotopic B16F10 tumors (**H**) from WT and *Plxna4* KO tumor-bearing mice. LLC tumor growth (**I**) and tumor weight (**J**) of lethally irradiated WT mice reconstituted with WT (WT→WT) or *Plxna4* KO (KO→WT) BM cells. Tumor growth (**K**) and tumor weight (**L**) in an orthotopic E0771 breast cancer model. Flow cytometric analysis of CTLs in the tdLNs (**M**) and primary tumor (**N**) from WT→WT and *Plxna4* KO→WT chimeras. For the *in vivo* experiments, $n = 4$–8 mice per group. *, $P < 0.05$; **, $P < 0.01$; ***, $P < 0.001$; and ****, $P < 0.0001$ versus WT (**A**–**D**, **G,** and **H**), CTLs in the tumor border (**F**) and versus WT→WT (**I**–**N**). All graphs show mean ± SEM.

sorted TAMs from WT and *Plxna4* KO tumor-bearing mice (Supplementary Fig. S1I), suggesting that, at least in these conditions, *Plxna4* is not required for macrophage localization or polarization within the TME.

Plxna4 was described as a negative regulator of T-cell–mediated immune responses (18, 24), so we therefore investigated if the tumor-suppressing phenotype observed in *Plxna4* KO mice was related to T-cell functions. Flow cytometric analysis showed that tumor-bearing *Plxna4* KO versus WT mice had increased numbers of CTLs in the tdLNs (**Fig. 1C**; Supplementary Fig. S1J). Histologically, we found that mice lacking *Plxna4* had increased infiltration of CTLs into the core of the tumor when compared with WT mice (**Fig. 1D**). Paired analysis of CTLs in the outer area versus the inner area of the same tumor suggested that, compared with their WT counterparts, *Plxna4* KO CTLs had increased capacity of migrating from the outer rim into the core of the tumor (**Fig. 1E** and **F**). Therefore, we hypothesized that *Plxna4* KO CTLs subvert a Plxna4-dependent T-cell exclusion mechanism seen in WT mice. Consistently, in an orthotopic B16F10 melanoma model, we observed a higher infiltration of CTLs, in both the tdLN (**Fig. 1G**) and primary tumor (**Fig. 1H**) of *Plxna4* KO versus WT mice. When looking more closely into the different $CD8^+$ T-cell subsets (naïve, central memory, effector/memory, and terminally exhausted T cells), the proportion of each $CD8^+$ T-cell subset in both the tdLNs and tumors remained the same in *Plxna4* KO versus WT

mice (Supplementary Fig. S1K and S1L). Conversely, in both tumor models, total $CD4^+$ T cells did not change, either in numbers (Supplementary Fig. S1M–S1P) or in their localization within the TME (Supplementary Fig. S1Q and S1R).

To further restrict the KO of Plxna4 to the immune system, we generated BM chimeras by transplanting BM cells from WT or *Plxna4* KO mice into lethally irradiated WT recipient mice, WT→WT and *Plxna4* KO→WT, respectively. Upon reconstitution, *Plxna4* KO→WT chimeras displayed normal blood counts, comparable with those of WT→WT mice (Supplementary Table S7). Upon subcutaneous engraftment, LLC tumor growth in *Plxna4* KO→WT chimeras was slower than in WT→WT chimeras (**Fig. 1I** and **J**), resembling our results in *Plxna4* KO mice (**Fig. 1A** and **B**). In an alternative tumor model, obtained by the orthotopic injection of E0771 breast cancer cells, tumor progression was significantly decreased upon deletion of *Plxna4* in the BM (**Fig. 1K** and **L**). Similar to *Plxna4* KO mice, higher numbers of CTLs, but not of $CD4^+$ T cells, were found in both the tdLN (**Fig. 1M**; Supplementary Fig. S1S) and primary tumor (**Fig. 1N**; Supplementary Fig. S1T) in *Plxna4* KO→WT compared with WT→WT chimeras. Altogether, these results show that a *Plxna4*-deficient tumor stroma or immune system results in impaired tumor growth and in the selective increase of CTLs inside both the tdLN and the tumor core.

Plxna4 expression is dynamically regulated in CTLs

Elevated CTL infiltration in the TME correlates with a good prognosis in several tumor types (4). Because we detected higher CTL numbers in the tumor core of *Plxna4* KO mice (**Fig. 1D**, **H**, and **N**), we investigated the direct role of *Plxna4* in these cells. First, we observed that *Plxna4* expression was upregulated in activated CTLs upon 3 days of anti-CD3/CD28 stimulation *in vitro* (**Fig. 2A**). Purified $CD4^+$ T cells showed similar kinetics of *Plxna4* expression, but at about one third the abundance of CTLs, both in the naïve and active state (**Fig. 2A**). In line with regulation at the transcript level, protein staining revealed that the number of Plxna4-expressing activated CTLs was increased compared with naïve cells (**Fig. 2B**). Similar to murine data, the expression of *PLXNA4* in human T cells was also upregulated upon later stages of T-cell activation, and this to a greater degree in CTLs than in $CD4^+$ T cells (**Fig. 2C**). On the basis of these observations, we characterized the expression of *Plxna4* in CTLs sorted from the circulation of healthy or tumor-bearing mice. Compared to healthy mice, *Plxna4* was upregulated in CTLs in both an orthotopic melanoma model (B16F10) and a subcutaneous LLC lung cancer model (**Fig. 2D**). *Plxna4* was also upregulated in circulating CTLs after mouse infection with a LCMV-OVA, which has a specific tropism for dendritic cells (Supplementary Fig. S2A; ref. 19). These data suggest an involvement of Plxna4 in CTLs upon antigen recognition.

To assess the relation between Plxna4 expression, activation status and tissue of origin, we sorted different $CD8^+$ T cell subsets from the blood and LNs in healthy mice (Supplementary Fig. S2B), or from the blood, tdLN, and tumor tissue in B16F10 tumor–bearing mice (Supplementary Fig. S2C). In healthy mice, *Plxna4* was expressed in all the circulating T-cell subsets, but it was decreased in effector/memory T cells or undetectable in naïve and central memory T cells sorted from the LNs (**Fig. 2E**). In B16F10 tumor–bearing mice, *Plxna4* abundance in circulating naïve and central memory T cells were comparable with those measured in healthy mice but was strongly augmented in circulating effector/memory T cells, which have encountered the antigen in the tdLNs and consequently express CD44 (**Fig. 2F**). However, in the tdLNs or in the tumor bed, *Plxna4* expression in effector/memory T cells was reduced and was undetectable in naïve, central memory, and exhausted CTLs, the latter being the most abundant subset in the tumor bed (**Fig. 2F**; Supplementary Fig. S2C). Altogether, our data suggest that T-cell activation increases *Plxna4* in effector/memory CTLs, but this expression is downregulated in all T-cell subsets when entering the inflammatory site. These observations held also true in a liver inflammation model, induced by HDI of a plasmid directing the expression of OVA (25). In this model, circulating antigen-primed $CD8^+CD44^{Hi}$ T cells expressed more *Plxna4* than their naïve $CD44^{Lo}$ counterparts (**Fig. 2G**). Similar to what was observed in tumor-infiltrating CTLs (**Fig. 2F**), *Plxna4* expression was also halved in $CD8^+CD44^{Hi}$ T cells infiltrating inflamed livers (**Fig. 2G**). Altogether, these data show that *Plxna4* expression is induced in effector/memory CTLs upon T-cell activation and sustained in circulation, while reduced at the inflammatory sites.

Genetic knockout of *Plxna4* in CTLs increases their motility and proliferation via enhanced Rac1 activity

As the expression of *Plxna4* in circulating CTLs was increased in tumor-bearing mice compared with healthy mice, but decreased upon their infiltration into the tumor bed (**Fig. 2D** and **F**), we studied the functional relevance of Plxna4 in CTLs. We analyzed the proliferation of WT and *Plxna4* KO CTLs in an *in vitro* time course experiment. From day 3 of activation, *Plxna4* KO CTLs showed a higher proliferation rate than WT cells (**Fig. 3A** and **B**; Supplementary Fig. S3A). This difference in proliferation was increasing with time, reaching almost two-fold higher rate at day 5 of stimulation (**Fig. 3A**), consistent with the observation that *Plxna4* expression increases over time following stimulation (**Fig. 2A**). In contrast, the apoptotic rate of WT and *Plxna4* KO CTLs at different timepoints following stimulation did not change (Supplementary Fig. S3B). Downstream effector functions of *in vitro* activated CTLs were also not affected, because the analysis of IFNγ and granzyme B (GrzmB) expression did not show any differences between WT and *Plxna4* KO CTLs (Supplementary Fig. S3C–S3F). Unlike CTL proliferation, expansion of activated $CD4^+$ T cells did not change significantly between WT and *Plxna4* KO T cells (Supplementary Fig. S3G).

Given the increased numbers of *Plxna4* KO CTLs in the tdLNs (**Fig. 1C**, **G**, and **M**) and in the primary tumor site (**Fig. 1D**, **H**, and **N**), we questioned whether chemotaxis could also be affected. *In vitro* transwell migration assays, in the presence of CCL21 and CCL19, chemokines involved in T-cell homing to the LNs (26), or CXCL9 and CXCL10, chemokines involved in T-cell homing to tumors (27), showed that *Plxna4* KO CTLs had increased migratory capacity than WT cells (**Fig. 3C** and **D**), whereas $CD4^+$ T-cell migration did not change (Supplementary Fig. S3H). The surface abundance of the CCL21 and CCL19 receptor CCR7 in naïve CTLs, or the CXCL9 and CXCL10 receptor CXCR3 in activated CTLs, were comparable in both genotypes (Supplementary Fig. S3I and S3J). However, transwell migration assays with naïve CTLs, treated with anti-CCR7, and activated CTLs, treated with anti-CXCR3, demonstrated reduced migration of *Plxna4* KO CTLs (**Fig. 3E** and **F**). This suggests that the increased migration potential of *Plxna4* KO CTLs is dependent on chemokine receptor signaling. Because the intracellular portion of *Plxna4* contains a GTPase-activating protein (GAP) domain with a Rho GTPase-binding domain insert (28), and Rac1, a member of the Rho small GTPases family, is necessary for the correct homing of T cells to the LNs (29), we hypothesized that *Plxna4* could regulate the activation of small GTPases in CTLs. We performed a GTPase pull-down assay to measure GTP-bound Rac1 in both WT and *Plxna4* KO activated CTLs. Compared with WT, *Plxna4* KO T cells had

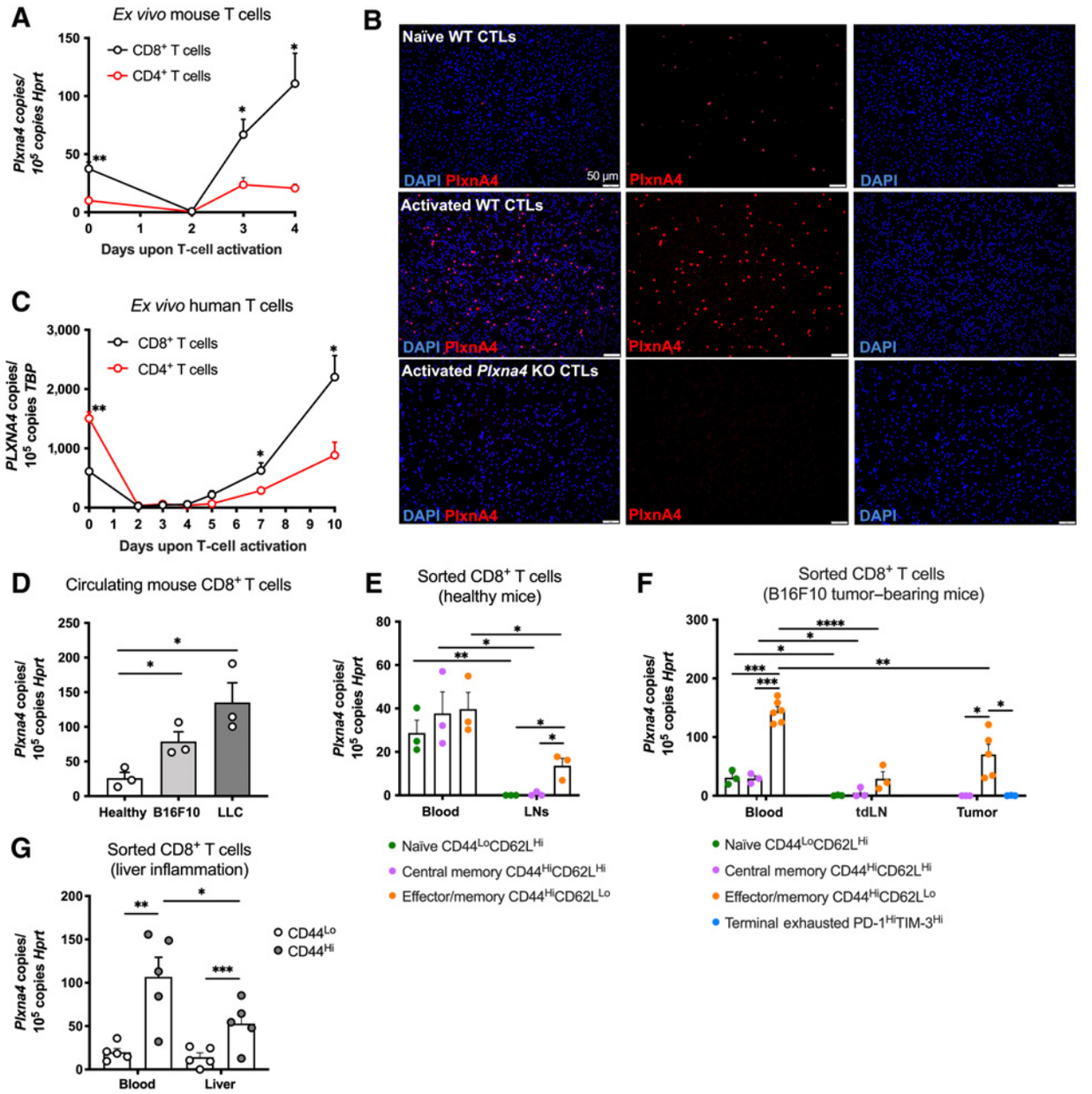

Figure 2.

Plxna4 expression is dynamically regulated in CTLs. **A,** Time course of *Plxna4* expression in purified mouse CD8$^+$ and CD4$^+$ T cells activated with anti-CD3/CD28 for 3 days and further expanded in the presence of IL2. **B,** Representative images of Plxna4 cytospin staining on WT and *Plxna4* KO CTLs before and after 3 days of anti-CD3/CD28 activation (scale bar, 50 μm). **C,** Time course of *Plxna4* expression in purified human CD8$^+$ and CD4$^+$ T cells activated with anti-CD3/CD28 for 3 days and further expanded in the presence of IL2. **D,** *Plxna4* expression in circulating CTLs sorted from healthy mice and orthotopic B16F10 or subcutaneous LLC tumor–bearing mice. **E,** *Plxna4* expression in naïve T cells (CD8$^+$CD44^{Lo}CD62L^{Hi}), effector/memory T cells (CD8$^+$CD44^{Hi}CD62L^{Lo}), and central memory T cells (CD8$^+$CD44^{Hi}CD62L^{Hi}) sorted from the circulation and LNs of healthy mice. **F,** *Plxna4* expression in naïve T cells (CD8$^+$CD44^{Lo}CD62L^{Hi}), effector/memory T cells (CD8$^+$CD44^{Hi}CD62L^{Lo}), central memory T cells (CD8$^+$CD44^{Hi}CD62L^{Hi}), and terminally exhausted T cells (CD8$^+$PD-1^{Hi}TIM-3^{Hi}) sorted from the circulation, tdLNs, and B16F10 orthotopic tumors of tumor-bearing mice. **G,** *Plxna4* expression in CD8$^+$CD4^{Lo} and CD8$^+$CD44^{Hi} T cells sorted from the circulation and liver of hydrodynamically vaccinated mice. For the *in vivo* experiments, $n = 3$–5 mice per group (**D**–**G**). *In vitro* results (**A** and **C**) were performed in triplicates and are representative of two independent experiments. *, $P < 0.05$; **, $P < 0.01$; and ***, $P < 0.001$ versus naïve and activated mouse CD4$^+$ T cells (**A**), naïve and activated CD4$^+$ human T cells (**C**), circulating CTLs in healthy mice (**D**), effector/memory T cells in LNs or corresponding circulating T-cell subset (**E**), effector/memory T cells present in the same tissue or corresponding circulating T-cell subset (**F**), circulating CD8$^+$CD44^{Hi} T cells, and CD8$^+$CD44^{Hi} T cells in the liver (**G**). All graphs show mean ± SEM.

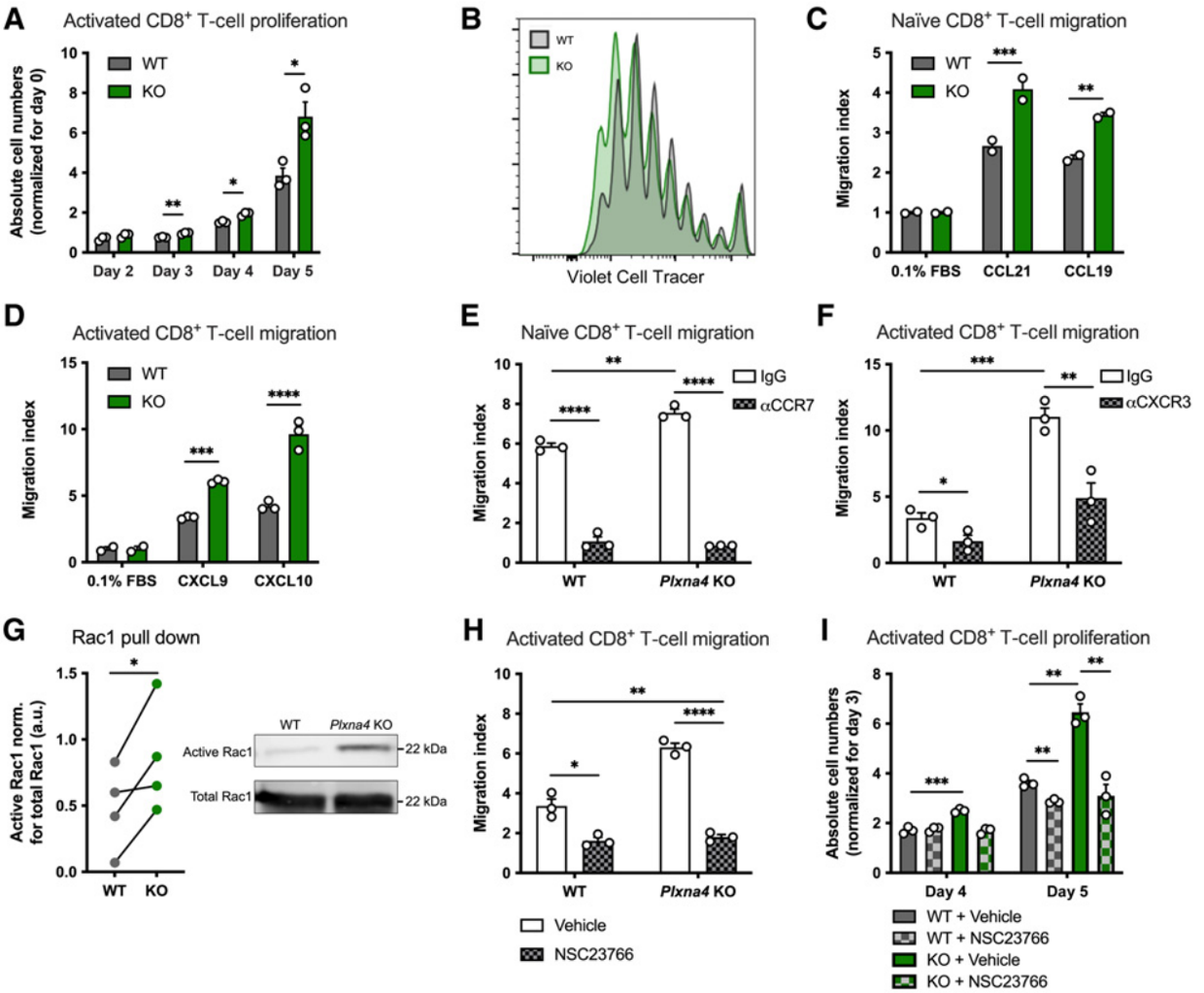

Figure 3.

Genetic knockout of *Plxna4* in CTLs increases motility and proliferation via enhanced Rac1 activity. *In vitro* proliferation of WT and *Plxna4* KO CTLs upon anti-CD3/CD28 activation showing absolute cell numbers (**A**) and a representative histogram (**B**) of Violet Cell Tracer fluorescence intensity, gated on $CD8^+$ T cells, after 4 days in culture. **C,** Transmigration assay of naïve WT and *Plxna4* KO CTLs toward CCL21 and CCL19 chemokines. **D,** Transmigration assay of activated WT and *Plxna4* KO CTLs toward CXCL9 and CXCL10 chemokines. **E,** Transmigration assay of naïve WT and *Plxna4* KO CTLs toward the CCL21 chemokine, treated with IgG or anti-CCR7. **F,** Transmigration assay of activated WT and *Plxna4* KO CTLs toward the CXCL10 chemokine, treated with IgG or anti-CXCR3. **G,** GTP-bound Rac1 pull-down assay on activated WT and *Plxna4* KO CTLs. Quantification by densitometry, paired analysis on each individual experiment (left) and a representative image of the Western blot analysis (right). **H,** Transmigration assay of activated WT and *Plxna4* KO CTLs toward the CXCL10 chemokine, treated with either vehicle or the Rac1 inhibitor NSC23766. **I,** *In vitro* proliferation of activated WT and *Plxna4* KO CTLs, treated at day 3 with either vehicle or the Rac1 inhibitor NSC23766. *In vitro* results were performed in triplicates (**A**, **D**–**F**, **H**, and **I**) or duplicates (**C**) and are representative of at least two independent experiments. Pull-down assay (**G**) is represented as the pooled data from four independent experiments (left), and the Western blot analysis is representative of at least three independent experiments (right). *, $P < 0.05$; **, $P < 0.01$; ***, $P < 0.001$; and ****, $P < 0.0001$ versus WT CTLs (**A**, **C**, and **D**), IgG-treated WT and *Plxna4* KO CTLs (**E** and **F**), and vehicle-treated WT and *Plxna4* KO CTLs (**H** and **I**). All graphs show mean ± SEM.

an increased amount of active (GTP-bound) Rac1 (**Fig. 3G**). The amount of GTP-bound Rap1, however, was similar between both conditions (Supplementary Fig. S3K and S3L). In line with the previously reported involvement of Rac1 in CTL migration and proliferation (30), pharmacologic Rac1 inhibition on activated CTLs was sufficient to reduce migration and proliferation of both *Plxna4* WT and KO cells (**Fig. 3H** and **I**). The latter suggests that active Rac1 is required for the phenotype observed in *Plxna4* KO CTLs.

Plxna4 KO CTLs show increased homing and proliferation capacity in inflammatory sites

To assess the *in vivo* role of *Plxna4* on CTL migration and proliferation, we performed competition assays in which WT and *Plxna4* KO CTLs, either naïve (LN-homing) or *in vitro* preactivated (inflamed tissue-homing), were coinjected i.v. into mice. When naïve WT and *Plxna4* KO CTLs were transferred into healthy WT mice, *Plxna4* KO CTLs were more efficient in reaching the LNs (**Fig. 4A** and **B**; Supplementary Fig. S4A and S4B). Both WT and *Plxna4* KO

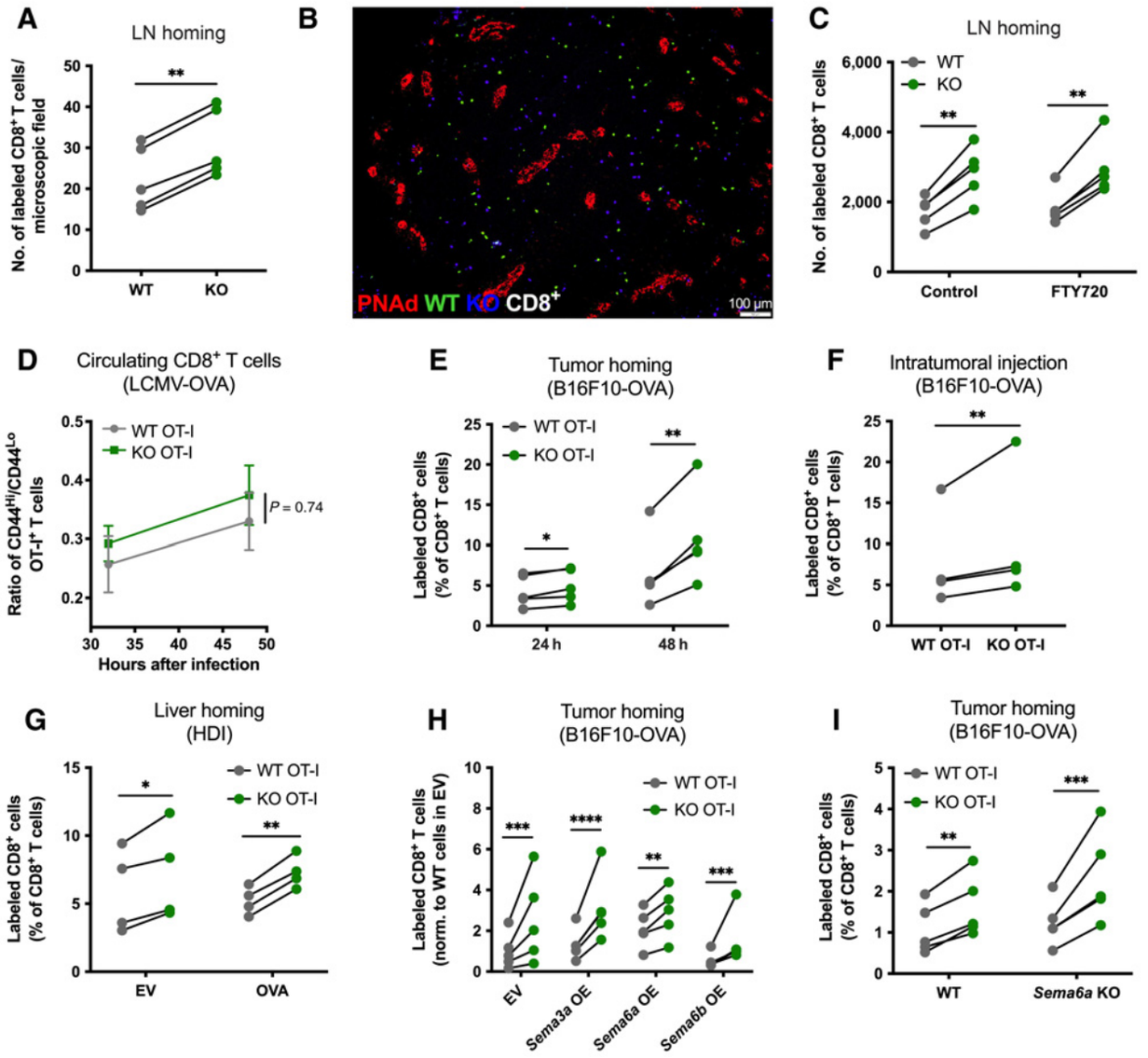

Figure 4.

Plxna4 KO CTLs show increased homing and proliferation capacity in inflammatory sites. Homing of naïve WT and *Plxna4* KO CTLs to the LNs of healthy mice quantified by histology (**A**) and representative micrograph (scale bar, 100 µm; **B**). **C,** Homing of naïve WT and *Plxna4* KO CTLs to the LNs of healthy mice treated with either vehicle or the S1PR inhibitor FTY720. **D,** Ratio of $CD8^+CD44^{Hi}$ to $CD8^+CD44^{Lo}$ circulating WT and *Plxna4* KO OT-I T cells in mice 32 hours and 48 hours after LCMV-OVA infection, analyzed by flow cytometry. **E,** Tumor homing of activated WT and *Plxna4* KO OT-I T cells in B16F10-OVA tumor–bearing mice assessed by flow cytometry 24 hours and 48 hours after tail vein injection. **F,** Flow cytometric analysis of labeled T cells in B16F10-OVA tumors 24 hours after intratumoral injection of activated WT and *Plxna4* KO OT-I T cells. **G,** Liver homing of activated WT and *Plxna4* KO OT-I T cells in mice hydrodynamically injected with empty vector (EV) or ovalbumin vector (OVA). **H,** Tumor homing of activated WT and *Plxna4* KO OT-I T cells in tumor-bearing mice, injected with B16F10-OVA cancer cells transduced with EV or overexpressing (OE) *Sema3a*, *Sema6a*, or *Sema6b*. T-cell infiltration was assessed by flow cytometry 24 hours after tail vein injection. **I,** Tumor homing of activated WT and *Plxna4* KO OT-I T cells in WT and *Sema6a* KO tumor-bearing mice, injected with B16F10-OVA cancer cells. T-cell infiltration was assessed by flow cytometry 24 hours after tail vein injection. For the *in vivo* experiments, $n = 4$–5 mice per group. *, $P < 0.05$; **, $P < 0.01$; ***, $P < 0.001$; and ****, $P < 0.0001$ versus WT CTLs (**A** and **C**) and WT OT-I T cells (**E–I**). All graphs show mean ± SEM.

CTLs were able to enter the paracortical areas of the LNs without entrapment in the high endothelial venules (HEV; **Fig. 4B**). To evaluate whether increased detection of *Plxna4* KO CTLs was due an inability to exit the LNs, we treated WT mice with fingolimod (FTY720), an immunomodulatory drug that inhibits lymphocyte egress from lymphoid tissues by downregulating sphingosine-1 phosphate receptor (S1PR; ref. 31). Treatment with FTY720 entrapped both WT and *Plxna4* KO CTLs in the LNs, but *Plxna4* KO CTLs were still present in higher numbers in the LNs compared with WT controls (**Fig. 4C**). To further investigate if *Plxna4* deficiency would affect T-cell egression from the LNs, we generated WT and *Plxna4* KO OT-I T cells, expressing a TCR which specifically recognizes the OVA peptide presented in MHC class I. Thereafter, we took advantage of the LCMV-OVA model, where infected dendritic cells present the

OVA peptide in MHC class I (19). Following the systemic injection of naïve WT or *Plxna4* KO OT-I T cells in LCMV-OVA–infected mice, we calculated the ratio between antigen-primed $CD44^{Hi}$ and naïve $CD44^{Lo}$ WT or *Plxna4* KO OT-I T cells in circulation over time. In this way, we found that similar numbers of $CD44^{Hi}$ *Plxna4* KO OT-I T cells were released into the blood 16 hours earlier than $CD44^{Hi}$ WT OT-I T cells but their speed of egression (graphically represented by the slope of the line) was the same (**Fig. 4D**). This observation suggests that the exit from the LNs of activated *Plxna4* KO CTLs was not altered but only anticipated due to their faster arrival into the LN.

Next, we studied the biological functions of Plxna4 in CTLs within the tumor or other sites of inflammation. In competition assays, we found increased tumor homing of *Plxna4* KO versus WT OT-I T cells 24 hours after their systemic coinjection in mice bearing OVA-expressing B16F10 (**Fig. 4E**) or LLC tumors (Supplementary Fig. S4C). To differentiate if the increased number of *Plxna4* KO CTLs in the tumor was a consequence of increased migratory/infiltrative capacity or higher proliferative ability, as observed *in vitro* (**Fig. 3A** and **B**), we followed OVA-expressing melanoma tumors for an additional 24 hours. Forty-eight hours after systemic injection of OT-I T cells, the ratio between *Plxna4* KO/WT OT-I T cells in the tumor bed was higher compared with what was calculated at 24 hours (**Fig. 4E**; Supplementary Fig. S4D), suggesting that the increased intratumoral accumulation of *Plxna4* KO CTLs was the result of both augmented migration and proliferation. The fluorescent probe labelling *Plxna4* KO tumor-infiltrating OT-I T cells was more diluted than in WT OT-I cells 24 hours after the systemic coinjection of activated WT and KO CTLs (Supplementary Fig. S4E), further suggesting a higher proliferation rate of *Plxna4* KO CTLs. To control for potential differential recruitment, we coinjected activated WT and *Plxna4* KO OT-I T cells intratumorally in B16F10-OVA tumors and observed increased proliferation in cells lacking *Plxna4* (**Fig. 4F**). Then, we assessed if the loss of *Plxna4* could confer both a migratory and proliferative advantage in other inflammatory conditions as well. To this end, we used the HDI model described above and found that *in vitro* activated *Plxna4* KO OT-I T cells infiltrated the inflamed livers more efficiently than WT OT-I T cells (**Fig. 4G**). This effect was more evident when hepatocytes were forced to express OVA (**Fig. 4G**; Supplementary Fig. S4F and S4G), which would boost proliferation as well. Taken together, these results suggest that *Plxna4* deletion in CTLs increases both their migratory/infiltrative capacity and proliferation rate in response to TCR activation.

Finally, we evaluated whether infiltrating CTLs were attracted or repulsed by interactions *in trans* with semaphorins expressed in the TME. To this end, B16F10-OVA cancer cells overexpressing the most relevant Plxna4 ligands (*Sema3a*, *Sema6a*, or *Sema6b*) were injected in WT mice (Supplementary Fig. S4H–S4J). Consistent with our previous observations (**Fig. 4E**), 24 hours after systemic injection, *Plxna4* KO OT-I T cells were more efficient in infiltrating melanoma tumors transduced with a mock empty vector (**Fig. 4H**). This finding held true even when the tumors overexpressed *Sema3a*, *Sema6a*, or *Sema6b* (**Fig. 4H**). Moreover, the increased homing capacity of *Plxna4* KO versus WT OT-I T cells was also seen in *Sema6a* KO tumor-bearing mice (**Fig. 4I**). Ruling out the engagement of *Sema6a* presentation by T cells themselves, activated *Sema6a* KO CTLs did not mimic *Plxna4* deficiency in terms of *in vitro* migration towards CXCL10, but rather showed the same chemotaxis as observed in WT cells (Supplementary Fig. S4K). Altogether, these findings suggest that presentation of semaphorins by the host (or autocrine signals by *Sema6a*) do not affect CTL infiltration and provide evidence for another nonconventional Plxna4-dependent but semaphorin-independent mechanism controlling CTL motility in cancer.

Adoptive transfer of *Plxna4* KO CTLs shows improved antitumor efficacy in a melanoma model

Prompted by our observations that Plxna4 functions as a negative regulator of CTL proliferation and migration, we evaluated if the deletion of *Plxna4* in CTLs was sufficient to increase antitumor immunity in the context of ACT. As a proof of concept of immunotherapeutic validation of *Plxna4* deficiency in CTLs, we first injected naïve WT or *Plxna4* KO OT-I T cells i.v. into LLC-OVA lung and B16F10-OVA melanoma tumor–bearing WT recipient mice. Mice receiving *Plxna4* KO OT-I T cells displayed a higher degree of tumor inhibition (Supplementary Fig. S5A and S5B), pointing to a direct effect of *Plxna4* deficiency in CTL activity. Secondly, consistent with a therapeutic approach, activated OT-I T cells were transferred into the circulation of B16F10-OVA tumor-bearing WT recipient mice. In this setting, *Plxna4* KO OT-I T cells exerted increased antitumor effects than their WT counterparts, as demonstrated by decreased tumor growth and weight (**Fig. 5A**–**C**). As expected, WT CTLs were also able to control tumor growth, but to a lesser extent than *Plxna4* KO OT-I T cells (**Fig. 5A**–**C**). When we analyzed the number of tumor-infiltrating CTLs 4 days after ACT, melanoma tumors that received *Plxna4* KO OT-I T cells contained an increased number of intratumoral OT-I T cells compared with the ones treated with WT OT-I cells (**Fig. 5D**). Nevertheless, these cells showed no difference in cytotoxicity, evaluated by their expression of IFNγ and GzmB after T-cell restimulation *ex vivo* (Supplementary Fig. S5C and S5D). In this model of ACT, the administration of *Plxna4* KO OT-I T cells also extended overall survival when compared with the adoptive transfer of WT OT-I T cells (**Fig. 5E**). Taken together, these data demonstrate that *Plxna4* deletion in CTLs is sufficient to increase antitumor immunity in a conventional ACT setting and that targeting of Plxna4 might thus be a valuable strategy to improve CTL infiltration.

Potential clinical relevance of *Plxna4* in CTLs in patients with melanoma

To translate our findings to human cancer, we analyzed *PLXNA4* expression in circulating CTLs in a cohort of patients with metastatic melanoma (Supplementary Table S3). Similar to our observations in a murine model (**Fig. 2**), CTLs isolated from the peripheral blood of patients with melanoma expressed higher quantities of *PLXNA4*, but not of other type-A plexins, compared with those measured in circulating CTLs from healthy donors (**Fig. 6A**; Supplementary Fig. S6A–S6C). *PLXNA4* abundance was also higher in circulating $CD4^+$ T cells isolated from the same patients (Supplementary Fig. S6D). In contrast, expression of *PLXNA4* in circulating monocytes isolated from both healthy volunteers and patients across different tumor types were low or undetectable (Supplementary Fig. S6E; Supplementary Table S5).

We then analyzed *Plxna4* expression in circulating CTLs of patients with melanoma prior to and after the first cycle of ICI therapy (anti–PD-1 alone or in combination with anti–CTLA-4). We observed a significant decrease of *Plxna4* in CTLs following treatment (**Fig. 6B**). When stratifying these patients for their clinical response to ICI therapy, we found that the decrease in *Plxna4* expression in circulating CTLs was significant in the responders but not in the nonresponders (**Fig. 6C** and **D**).

On the basis of these clinical data, we speculated that the benefit from ICI therapy may depend, at least partly, on the downregulation of

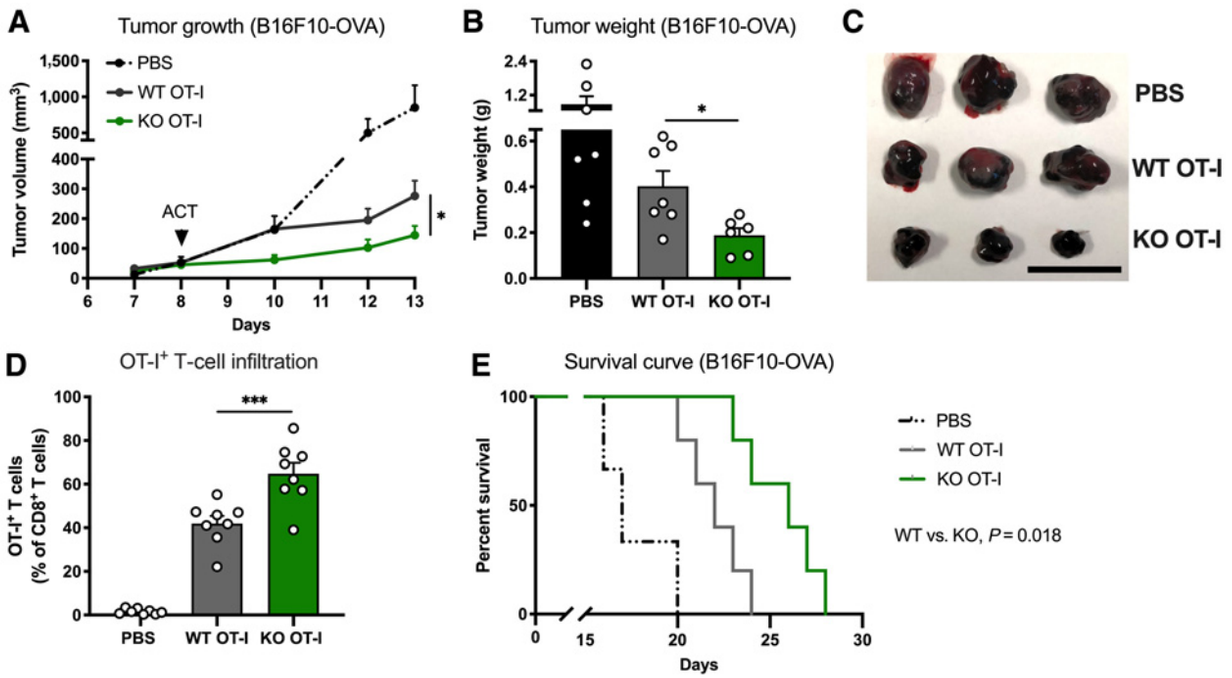

Figure 5.

Adoptive transfer of *Plxna4* KO CTLs leads to improved antitumor immunity. Tumor growth (**A**), tumor weight (**B**), and representative images (**C**) of end-stage tumors following adoptive transfer (ACT) of activated WT and *Plxna4* KO OT-I T cells in B16F10-OVA tumor–bearing WT mice (scale bar, 2 cm). **D,** Flow cytometric analysis of intratumoral OT-I$^+$ T cells in B16F10-OVA tumors isolated 4 days after ACT. **E,** Kaplan–Meier overall survival curves. For the *in vivo* experiments, $n = 6$–8 mice per group. *, $P < 0.05$; ***, $P < 0.001$ versus WT OT-I T cells. All graphs show mean ± SEM.

Plxna4. This hypothesis was tested by treating B16F10 tumor–bearing mice with anti–PD-1 for a week, resulting in a reduction of *Plxna4* expression in circulating CTLs compared with IgG-treated tumor-bearing mice (**Fig. 6E**). This downregulation of *Plxna4* expression upon anti–PD-1 blockade was also true for *in vitro* activated human CTLs, but not for CD4$^+$ T cells (**Fig. 6F**). The hypothesis that PD-1 blockade acts partly, but not only, through the downregulation of *Plxna4* in CTLs was also suggested by our findings that anti–PD-1 therapy in combination with ACT of WT OT-I cells reached a similar extent of tumor inhibition as observed with the transfer of *Plxna4* KO OT-I T cells alone (**Fig. 6G**). Perhaps by means of Plxna4-unrelated mechanisms of anti–PD-1, such as unleashing the PI3K–Akt pathway (32), the combination of *Plxna4* KO OT-I ACT and anti–PD-1 therapy led to an even stronger reduction in tumor growth than with *Plxna4* KO OT-I ACT alone (**Fig. 6G**). Members of the Forkhead box O (FOXO) family of transcription factors (TF), which are activated downstream to PD-1 and upon persistent TCR stimulation (33, 34), are described to regulate *Plxna4* expression (35). When treating *in vitro* activated CTLs with CBX, an inhibitor of FOXO1, 3, 4, and 6 (36), we observed that *Plxna4* expression was reduced even further than upon anti–PD-1 treatment (**Fig. 6H**), providing initial support that FOXO TFs may promote *Plxna4* expression upon chronic TCR stimulation and PD-1 induction.

Discussion

In the last decade, immunotherapy has emerged as a promising therapeutic option for patients with cancer. The use of ICIs, in particular, has revolutionized the field, enabling durable control of previously highly refractory and aggressive cancers, such as melanoma and lung cancer. However, a significant percentage of patients—60% to 80%—still do not benefit from this strategy (37). One of the main factors hampering ICIs is the exclusion of CTLs from the tumor bed, making these tumors T-cell "cold". In this study, we show that targeting Plxna4 might represent a novel strategy to drive T-cell inflammation in T-cell nonenriched tumors. Our data show that Plxna4 is dynamically regulated in CTLs and that its absence promotes an increased proliferative and homing capacity to the tdLNs and the tumor bed, leading to a more effective antitumor response (**Fig. 6I**).

In our study, *Plxna4* deletion in the stroma reduced tumor growth by specifically enhancing CTL infiltration, while the phenotype of other stromal cells remained unaffected. Although Plxna4 was shown to play a role in macrophages in the context of cancer or other pathologic conditions (15–17), we observed that deletion of *Plxna4* was not sufficient to impact on macrophage localization and phenotype. *Plxna4* was also described as a negative regulator of CD4$^+$ T-cell immune responses in experimental autoimmune diseases (18, 24). In our models, *Plxna4* is expressed by CD4$^+$ T cells but at lower abundance than in CTLs. Moreover, neither the infiltration nor the distribution of *Plxna4* KO CD4$^+$ T cells within the tumor was altered, pointing to a function of *Plxna4* specifically in CTLs. Given the functional redundancy among class A plexins (17, 38), homologous receptors expressed in TAMs, CD4$^+$ T cells, or endothelial cells, such as Plexin-A1, could compensate for the absence of Plxna4. In contrast, Plxna4 is indispensable for the fine-tuning of CTL proliferation and migration.

In terms of expression, naïve T cells found in the LNs show undetectable transcription of *Plxna4* compared with circulating naïve T cells, suggesting that the downregulation of *Plxna4* is required for

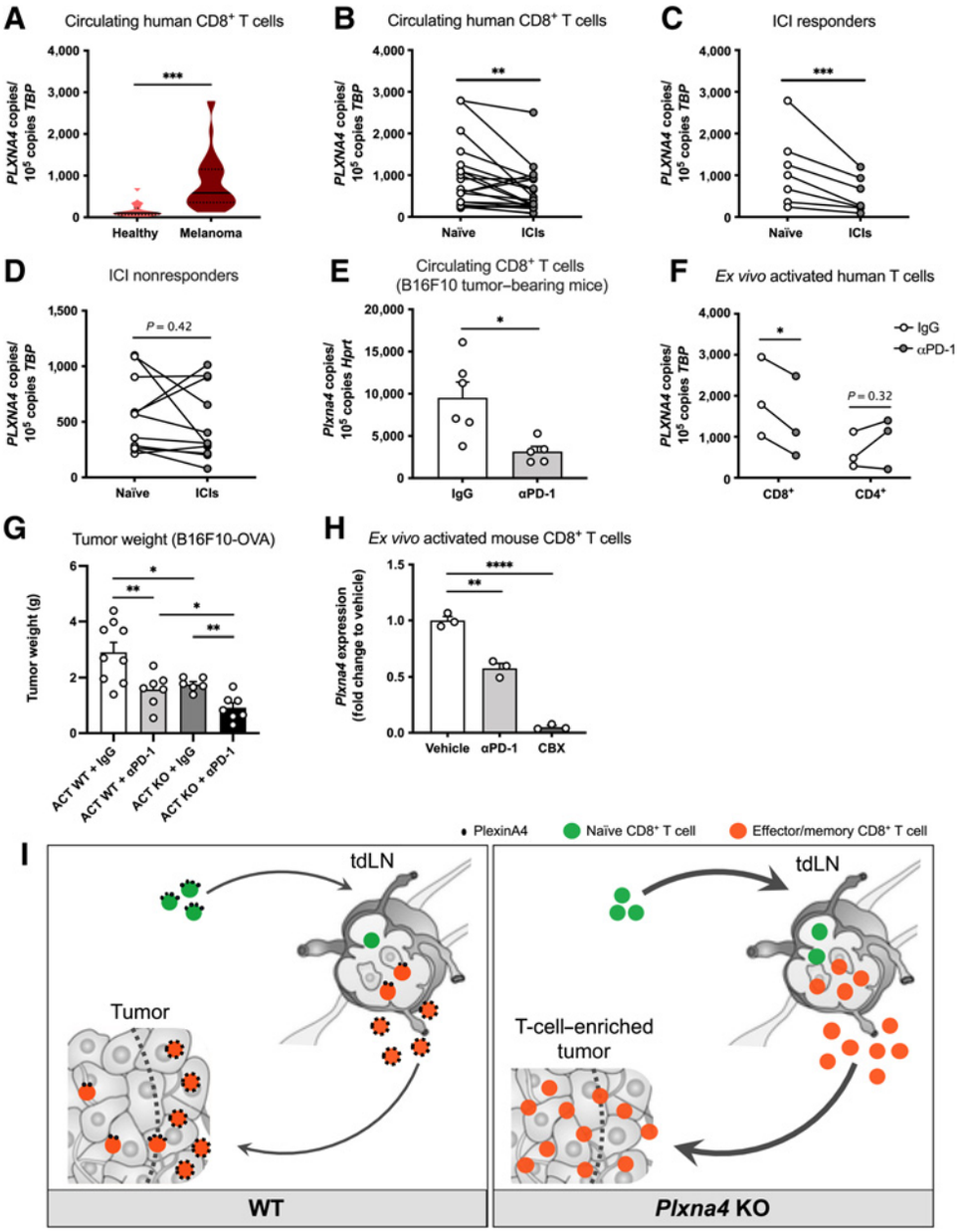

Figure 6.

PLXNA4 expression is upregulated in circulating CTLs of patients with metastatic melanoma. **A,** *PLXNA4* expression in isolated CTLs from the circulation of treatment-naïve melanoma patients versus healthy controls. **B,** Naïve versus paired ICI (anti–PD-1 alone or in combination with anti–CTLA-4)–treated melanoma patients 3 weeks after one cycle of treatment. *PLXNA4* expression in isolated CTLs from the circulation of treatment-naïve and paired ICI-treated patients with melanoma that clinically responded to ICIs (**C**) and patients with melanoma that did not respond to ICIs (**D**). **E,** *Plxna4* expression in circulating CTLs isolated from orthotopic B16F10 tumor–bearing mice treated with IgG or anti–PD-1. **F,** *PLXNA4* expression in *ex vivo* activated human $CD8^+$ and $CD4^+$ WT T cells treated with IgG or anti–PD-1. **G,** Weight of end-stage B16F10-OVA tumors receiving ACT of activated WT and *Plxna4* KO OT-I T cells in combination with IgG or anti–PD-1 therapy. **H,** Fold change of *Plxna4* expression in *ex vivo* activated mouse CTLs treated with vehicle, anti–PD-1, or CBX. **I,** Schematic overview of the data presented. For the patient data (**A**–**D**), $n = 16$ healthy controls, $n = 31$ treatment-naïve melanoma patients, and $n = 20$ ICI-treated patients with melanoma (see Supplementary Table S3). *In vitro* results (**F** and **H**) were performed in triplicates and are represented as the pooled data from two independent experiments. For the *in vivo* experiment (**E** and **G**), $n = 5$–9 mice per group. *, $P < 0.05$; **, $P < 0.01$; ***, $P < 0.001$; and ****, $P < 0.0001$ versus circulating CTLs in healthy individuals (**A**), circulating CTLs in treatment-naïve melanoma patients (**B** and **C**), circulating CTLs isolated from IgG-treated mice (**E**), IgG-treated human CTLs (**F**), B16F10-OVA tumors receiving ACT of activated WT OT-I T cells and IgG-treated B16F10-OVA tumors (**G**), and vehicle-treated mouse CTLs (**H**). All graphs show mean ± SEM.

CTLs to enter the lymphoid tissue. Indeed, homing of naïve *Plxna4* KO CTLs towards LNs of healthy mice was increased compared with WT CTLs. Upon T-cell activation, *Plxna4* transcripts were upregulated in CTLs in tumors, as well as in experimental models of liver inflammation or viral infection, demonstrating that different microenvironmental signals associated with inflammation, infections, or tumor progression can result in similar expression patterns, as described previously (39). In particular, Plxna4 protein expression was increased in CTLs activated *in vitro* when compared with their naïve counterpart, suggesting that Plxna4 is upregulated upon T-cell activation. Consistently, *Plxna4* transcription was specifically induced in the circulating effector/memory CTL fraction in tumor-bearing mice but reduced at inflammatory sites (cancer and liver), suggesting that *Plxna4* downregulation is required for their entry in these tissues. Indeed, genetic KO of *Plxna4* in activated CTLs increased their infiltration to both the tumor and the inflamed liver parenchyma. In addition, we hypothesized that higher *Plxna4* transcription observed in the pool of tumor-associated effector/memory T cells, compared with the undetectable levels in central memory and terminally exhausted T cells, was mainly reflecting the presence of Plxna4^{Hi} excluded T cells at the tumor border. In contrast, few Plxna4^{Lo} T cells enter the tumor core and proliferate when encountering tumor-associated antigens presented in MHC class I by the cancer cells or by tumor-infiltrating DCs (**Fig. 6I**). In line with this idea, tumor-bearing mice with stromal or hematopoietic *Plxna4* deletion had increased CTL numbers in the tumor core, which is likely the result of improved infiltration and proliferation in response to antigen repriming (**Fig. 6I**). This is also suggested by the fact that adoptive transfer of *in vitro* preactivated *Plxna4* KO CTLs exhibit increased homing and proliferation within OVA-overexpressing tumors. Altogether, it is reasonable to speculate that Plxna4 could work as a negative regulator of both naïve and effector/memory CTLs, by breaking their recruitment into the LNs and inflammatory sites. This mechanism is possibly mediated by the presence of proinflammatory, type I cytokines in these tissues (such as IL10, IFNγ, or others), which counter this break in a dynamic process and promote the downregulation of *Plxna4* and thus the entry and the proliferation of naïve CTLs in the LNs, and effector/memory CTLs in the inflamed tissue. However, in the context of cancer, this process fails to occur completely, possibly because the TME is enriched in anti-inflammatory, type II cytokines which impede the downregulation of *Plxna4* in effector/memory CTLs that are thus excluded at the border of the tumor. The concept of Plxna4 as a "break" of inflammatory processes agrees with previously published data showing that the absence of *Plxna4* exacerbates ongoing autoimmune diseases (18, 24) but does not result *per se* in the spontaneous development of autoimmune disorders or other pathologies, since *Plxna4* KO mice appear to be healthy (18, 22).

The intracellular portion of plexins contains GTPase-binding domains (28, 40), which can interact and negatively regulate Rac1, a Rho family GTPase involved in the modulation of the cytoskeleton (30, 41–43). Our data suggest that enhanced CTL migration in the absence of Plxna4 might be due to increased activation of Rac1, since we observed that *Plxna4* deficiency was associated with augmented GTP-bound Rac1, in line with what has been shown before in *Plxna4*-silenced endothelial cells (23). The modulation of Rac1 by Plxna4 is here functionally supported by the observation that treatment with the Rac1 inhibitor NSC23766 completely prevented the advantageous migration of *Plxna4* KO CTLs. Besides migration, CTL proliferation is also instrumental to mount a proper immune response (44). In this regard, *Plxna4* KO CTLs displayed increased proliferative capacity, arguing that Plxna4 negatively regulates CTL proliferation as well, akin to what has been suggested for *Plxna4* KO CD4$^+$ T cells in the context of autoimmune diseases (18). This increased proliferation can be attributed to enhanced Rac1 activity as well (30), as supported by our *in vitro* data comparing *Plxna4* WT and KO CTLs treated with Rac1 inhibitors. However, future work is warranted to assess if direct or indirect mechanisms are enrolled by Plxna4 to regulate Rac1 activation.

Given the repulsive activities propagated by Plxna4 when interacting with semaphorins (13, 14, 45), it may be attractive to hypothesize that the exclusion of CTLs from the tumor bed is a consequence of repulsive cues. However, our data illustrate that the overexpression in cancer cells of the most relevant Plxna4 ligands (*Sema3a*, *Sema6a*, and *Sema6b*), or the expression of the high-affinity ligand *Sema6a* in the TME and by T cells themselves, does not modulate CTL infiltration in the tumor bed. Because plexins are evolutionarily more conserved than semaphorins (46), we are tempted to believe that semaphorin-independent mechanisms are likely to be present in eukaryotic cells. Furthermore, we foresee that the inhibitory effect of Plxna4 on CTL expansion and chemotaxis is cell autonomous, and therefore independent of the interaction *in trans* of Plxna4 with semaphorins expressed in the TME. Of note, interactions *in cis* between plexins and transmembrane semaphorins, or other cell surface receptors, have been reported to modulate intracellular signaling and biological functions (45, 47–49). Thus, currently unknown interactions of Plxna4 with molecules coexpressed in T cells (other than *Sema6a*) could play a role in the observed phenotype, possibly by regulating Rac1 activation.

Our work suggests potential therapeutic and clinical implications. In an adoptive transfer setting, *Plxna4* KO CTLs outperformed WT cells in shrinking established B16F10 melanoma tumors, providing a proof of concept that Plxna4 targeting in CTLs facilitates antitumor immunity and could be integrated in existing cancer immunotherapy regimens. Because enforcing the trafficking of CTLs to malignant tissues can improve the efficacy of any immunotherapeutic regimens (50), and combination treatments are often needed to unleash a proper antitumor immune response (51), we believe that targeting Plxna4 also holds the potential to act synergistically with conventional immunotherapies, including ICIs. In our preclinical tumor models, ACT with *Plxna4* KO CTLs in combination with anti–PD-1 led to a more potent antitumor immune response compared with monotherapy, demonstrating a potential clinical value of Plxna4-targeted therapies. However, future studies should determine to which extent and with which implications on homeostatic immune control, the combined targeting of Plxna4 and other inhibitory receptors on CTLs can further increase the antitumor immune response.

Supporting our preclinical data, *Plxna4* expression was increased in circulating CTLs from patients with metastatic melanoma compared with healthy controls, further strengthening a possible translation of our mechanistic and therapeutic conclusions to human disease. Moreover, *Plxna4* expression in circulating CTLs was decreased after the first cycle of ICI therapy in melanoma patients that responded to the therapy. ICI therapy frequently leads to an increase in proliferation and migration of preexisting CTLs (52, 53), features related to the observed phenotype of *Plxna4* KO CTLs. This indicates that ICIs might partly work in circulation via the downregulation of Plxna4 in CTLs separately from previously characterized mechanisms (54). The expression of PD-1 (*Pdcd1*) is induced after TCR stimulation via members of the nuclear factor of activated T-cell (NFAT) family of transcription factors (55). Upon persistent antigen stimulation, PD-1 signaling inhibits multiple TCR downstream pathways and FOXO TFs are activated, further promoting *Pdcd1* transcription (33). Consistent with

Plxna4 being upregulated as a late activation marker, FOXOs are essential for activated T cells within days following primary TCR activation (33, 34). FOXOs are known to positively regulate several effector/memory functions such as T-cell homing and effector T-cell differentiation (56, 57), features that were all enhanced in *Plxna4* KO CTLs. Because we observed that FOXO TFs can regulate the expression of *Plxna4* (35), we speculate that later stages of T-cell activation are characterized by the upregulation of negative regulators of T-cell functions (immune checkpoint molecules), which include PD-1 itself but also the Plxna4 pathway. However, the link between FOXO transcription factors and expression of *Plxna4* remain incompletely defined and will need further investigation in future studies.

In terms of clinical management, biomarkers of tumor response to ICIs are needed to help guide treatment strategy. Our results suggest that expression of *PLXNA4* in circulating CTLs could be used as an early, noninvasive biomarker for monitoring patients' responses to immune checkpoint blockade. In line with our observations, changes in T-cell subsets of patients with metastatic melanoma were reported to occur within a short period after initiating ICI therapy (58). Although our CTL sampling was done in a prospective manner and larger cohorts of patients will be needed to further confirm our clinical results, the current data well-position *PLXNA4* expression in circulating CTLs as a potential biomarker of disease or response to immunotherapy.

Authors' Disclosures

W. Celus reports grants from Research Foundation Flanders during the conduct of the study. A.I. Oliveira reports grants from Research Foundation Flanders and personal fees from Fundação para a Ciência e a Tecnologia during the conduct of the study. A.D. Garg reports personal fees from Boehringer Ingelheim and Miltenyi Biotec outside the submitted work. M. Mazzone reports grants from Research Foundation Flanders, Fundação para a Ciência e a Tecnologia, FWO-Strategic Basic Research (SB) doctoral fellowship, Kom op tegen Kanker (Stand up to Cancer), the Flemish cancer society, FWO-Fundamental Research (FR) doctoral fellowship, fundamental postdoctoral mandate of the Belgian Foundation against Cancer (Stichting tegen Kanker), the FNRS, the Walloon Region, FWO, KU Leuven, Kom op Tegen Kanker, the Grand Challenges Program of VIB (which received support from the Flemish Government under the Management Agreement 2017-2021), the Northern Portugal Regional Operational Programme, European Regional Development Fund (ERDF), and ERC Consolidator Grants during the conduct of the study. W. Celus, A.I. Oliveira, and M. Mazzone report a patent for PCT application no. PCT/EP2020/064884 with title "$CD8^+$ T cells lacking plexins and their application in cancer treatment" issued, a patent for PCT application no. PCT/EP2020/064905 with title "Cancer treatment by targeting plexins in the immune compartment" issued, and a patent for PCT application no. PCT/EP2021/076314 with title "Biomarker for antitumor therapy" issued. No disclosures were reported by the other authors.

Authors' Contributions

W. Celus: Conceptualization, formal analysis, funding acquisition, validation, investigation, visualization, methodology, writing–original draft, writing–review and editing. **A.I. Oliveira:** Conceptualization, formal analysis, funding acquisition, validation, investigation, visualization, methodology, writing–original draft, writing–review and editing. **S. Rivis:** Validation, investigation. **H.H. Van Acker:** Validation, investigation. **E. Landeloos:** Resources. **J. Serneels:** Investigation; J. Serneels provided technical support. **S.T. Cafarello:** Investigation. **Y. Van Herck:** Resources. **R. Mastrantonio:** Investigation. **A. Köhler:** Investigation. **A.D. Garg:** Conceptualization. **V. Flamand:** Conceptualization. **L. Tamagnone:** Conceptualization. **J.C. Marine:** Conceptualization, resources. **M. Di Matteo:** Conceptualization, resources, methodology. **B.M. Costa:** Conceptualization. **O. Bechter:** Conceptualization, resources. **M. Mazzone:** Conceptualization, resources, data curation, supervision, funding acquisition, writing–original draft, project administration, writing–review and editing.

Acknowledgments

This work was supported by the Research Foundation Flanders (FWO; G0A8219N). A.I. Oliveira was supported by Fundação para a Ciência e Tecnologia (SFRH/BD/52287/2013) and by FWO under the project G0A8219N. W. Celus was supported by an FWO-Strategic Basic Research (SB) doctoral fellowship (1S26917N). S. Rivis was supported by an FWO-Fundamental Research (FR) doctoral fellowship (1197720N). H.H. Van Acker was supported by a fundamental postdoctoral mandate of the Belgian Foundation against Cancer (Stichting tegen Kanker). E. Landeloos was funded by Kom op tegen Kanker (Stand up to Cancer), the Flemish cancer society. A. Köhler and V. Flamand were funded by the FNRS (CDR 33685316 grant) and the Walloon Region (FEDER Wallonia-Biomed portfolio). A.D. Garg was supported by FWO (G0B4620N; EOS grant: 30837538), KU Leuven (C14/19/098; POR/16/040), and Kom op Tegen Kanker (KOTK/2018/11509/1). E. Landeloos, O. Bechter, and J.C. Marine are funded within the Grand Challenges Program of VIB, which received support from the Flemish Government under the Management Agreement 2017–2021 (VR 2016 2312 Doc.1521/4). B.M. Costa was supported by the Northern Portugal Regional Operational Programme (NORTE 2020) under the project NORTE-01–0145-FEDER-000013 and the European Regional Development Fund (FEDER) under the Portugal 2020 Partnership Agreement. M. Mazzone was granted by an ERC Consolidator Grant (773208) and by FWO (G0A8219N). The authors thank S. Willox, A. Tzoumpa, E. Achten, C. Serrano, J. Grieten, R. Tavares, and M. Cogels for their technical assistance. *Plxna4* KO mice were kindly offered by Dr. Castellani (Institut NeuroMyoGène, Université de Lyon, Lyon, France). *Sema6a* KO mice were kindly offered by Prof. Dr. Pasterkamp (Department of Translational Neuroscience, University Medical Center Utrecht, Utrecht, the Netherlands). LCMV-OVA virus was a kind gift from Prof. Dr. Pinschewer (University of Basel, Basel, Switzerland). Flow cytometry data were generated with the support from the VIB FACS Expertise Center.

The publication costs of this article were defrayed in part by the payment of publication fees. Therefore, and solely to indicate this fact, this article is hereby marked "advertisement" in accordance with 18 USC section 1734.

Note

Supplementary data for this article are available at Cancer Immunology Research Online (http://cancerimmunolres.aacrjournals.org/).

Received January 25, 2021; revised September 7, 2021; accepted November 16, 2021; published first November 23, 2021.

References

1. Chen DS, Mellman I. Oncology meets immunology: the cancer-immunity cycle. Immunity 2013;39:1–10.
2. Kruger S, Ilmer M, Kobold S, Cadilha BL, Endres S, Ormanns S, et al. Advances in cancer immunotherapy 2019 - latest trends. J Exp Clin Cancer Res 2019;38:268.
3. Galluzzi L, Chan TA, Kroemer G, Wolchok JD, Lopez-Soto A. The hallmarks of successful anticancer immunotherapy. Sci Transl Med 2018;10:eaat7807.
4. Fridman WH, Pages F, Sautes-Fridman C, Galon J. The immune contexture in human tumors: impact on clinical outcome. Nat Rev Cancer 2012;12:298–306.
5. Teng MW, Ngiow SF, Ribas A, Smyth MJ. Classifying cancers based on T-cell infiltration and PD-L1. Cancer Res 2015;75:2139–45.
6. Perala N, Sariola H, Immonen T. More than nervous: the emerging roles of plexins. Differentiation 2012;83:77–91.
7. He Z, Wang KC, Koprivica V, Ming G, Song HJ. Knowing how to navigate: mechanisms of semaphorin signaling in the nervous system. Sci STKE 2002; 2002:re1.
8. Kumanogoh A, Kikutani H. Immunologic functions of the neuropilins and plexins as receptors for semaphorins. Nat Rev Immunol 2013;13:802–14.
9. Capparuccia L, Tamagnone L. Semaphorin signaling in cancer cells and in cells of the tumor microenvironment–two sides of a coin. J Cell Sci 2009;122: 1723–36.
10. Suto F, Murakami Y, Nakamura F, Goshima Y, Fujisawa H. Identification and characterization of a novel mouse plexin, plexin-A4. Mech Dev 2003;120: 385–96.
11. Battistini C, Tamagnone L. Transmembrane semaphorins, forward and reverse signaling: have a look both ways. Cell Mol Life Sci 2016;73:1609–22.

12. Fujisawa H. Discovery of semaphorin receptors, neuropilin and plexin, and their functions in neural development. J Neurobiol 2004;59:24–33.
13. Suto F, Ito K, Uemura M, Shimizu M, Shinkawa Y, Sanbo M, et al. Plexin-A4 mediates axon-repulsive activities of both secreted and transmembrane semaphorins and plays roles in nerve fiber guidance. J Neurosci 2005;25: 3628–37.
14. Tawarayama H, Yoshida Y, Suto F, Mitchell KJ, Fujisawa H. Roles of semaphorin 6B and plexin-A2 in lamina-restricted projection of hippocampal mossy fibers. J Neurosci 2010;30:7049–60.
15. Wen H, Lei Y, Eun SY, Ting JP. Plexin-A4–semaphorin 3A signaling is required for Toll-like receptor- and sepsis-induced cytokine storm. J Exp Med 2010;207: 2943–57.
16. Kang S, Nakanishi Y, Kioi Y, Okuzaki D, Kimura T, Takamatsu H, et al. Semaphorin 6D reverse signaling controls macrophage lipid metabolism and anti-inflammatory polarization. Nat Immunol 2018;19:561–70.
17. Casazza A, Laoui D, Wenes M, Rizzolio S, Bassani N, Mambretti M, et al. Impeding macrophage entry into hypoxic tumor areas by Sema3a/Nrp1 signaling blockade inhibits angiogenesis and restores antitumor immunity. Cancer Cell 2013;24:695–709.
18. Yamamoto M, Suzuki K, Okuno T, Ogata T, Takegahara N, Takamatsu H, et al. Plexin-A4 negatively regulates T lymphocyte responses. Int Immunol 2008;20: 413–20.
19. Flatz L, Hegazy AN, Bergthaler A, Verschoor A, Claus C, Fernandez M, et al. Development of replication-defective lymphocytic choriomeningitis virus vectors for the induction of potent $CD8^+$ T-cell immunity. Nat Med 2010;16: 339–45.
20. Eisenhauer EA, Therasse P, Bogaerts J, Schwartz LH, Sargent D, Ford R, et al. New response evaluation criteria in solid tumors: revised RECIST guideline (version 1.1). Eur J Cancer 2009;45:228–47.
21. Hamm A, Prenen H, Van Delm W, Di Matteo M, Wenes M, Delamarre E, et al. Tumor-educated circulating monocytes are powerful candidate biomarkers for diagnosis and disease follow-up of colorectal cancer. Gut 2016;65:990–1000.
22. Yaron A, Huang PH, Cheng HJ, Tessier-Lavigne M. Differential requirement for Plexin-A3 and -A4 in mediating responses of sensory and sympathetic neurons to distinct class 3 Semaphorins. Neuron 2005;45:513–23.
23. Kigel B, Rabinowicz N, Varshavsky A, Kessler O, Neufeld G. Plexin-A4 promotes tumor progression and tumor angiogenesis by enhancement of VEGF and bFGF signaling. Blood 2011;118:4285–96.
24. Podojil JR, Chiang MY, Ifergan I, Copeland R, Liu LN, Maloveste S, et al. B7-H4 modulates regulatory $CD4^+$ T-cell induction and function via ligation of a semaphorin 3A/plexin-A4/neuropilin-1 complex. J Immunol 2018;201: 897–907.
25. Suda T, Liu D. Hydrodynamic gene delivery: its principles and applications. Mol Ther 2007;15:2063–9.
26. Girard JP, Moussion C, Forster R. HEVs, lymphatics, and homeostatic immune cell trafficking in lymph nodes. Nat Rev Immunol 2012;12:762–73.
27. Sackstein R, Schatton T, Barthel SR. T-lymphocyte homing: an underappreciated yet critical hurdle for successful cancer immunotherapy. Lab Invest 2017;97:669–97.
28. Kong Y, Janssen BJ, Malinauskas T, Vangoor VR, Coles CH, Kaufmann R, et al. Structural basis for plexin activation and regulation. Neuron 2016;91:548–60.
29. Faroudi M, Hons M, Zachacz A, Dumont C, Lyck R, Stein JV, et al. Critical roles for Rac GTPases in T-cell migration to and within lymph nodes. Blood 2010;116: 5536–47.
30. Gomez M, Tybulewicz V, Cantrell DA. Control of pre–T-cell proliferation and differentiation by the GTPase Rac-I. Nat Immunol 2000;1:348–52.
31. Morris MA, Gibb DR, Picard F, Brinkmann V, Straume M, Ley K. Transient T-cell accumulation in lymph nodes and sustained lymphopenia in mice treated with FTY720. Eur J Immunol 2005;35:3570–80.
32. Boussiotis VA. Molecular and biochemical aspects of the PD-1 checkpoint pathway. N Engl J Med 2016;375:1767–78.
33. Staron MM, Gray SM, Marshall HD, Parish IA, Chen JH, Perry CJ, et al. The transcription factor FoxO1 sustains expression of the inhibitory receptor PD-1 and survival of antiviral $CD8^+$ T cells during chronic infection. Immunity 2014; 41:802–14.
34. Delpoux A, Lai CY, Hedrick SM, Doedens AL. FOXO1 opposition of $CD8^+$ T-cell effector programming confers early memory properties and phenotypic diversity. Proc Natl Acad Sci U S A 2017;114:E8865–E74.
35. Paap RH, Oosterbroek S, Wagemans C, von Oerthel L, Schellevis RD, Vastenhouw-van der Linden AJA, et al. FoxO6 affects Plxna4-mediated neuronal migration during mouse cortical development. Proc Natl Acad Sci U S A 2016;113:E7087–E96.
36. Salcher S, Spoden G, Hagenbuchner J, Fuhrer S, Kaserer T, Tollinger M, et al. A drug library screen identifies Carbenoxolone as novel FOXO inhibitor that overcomes FOXO3-mediated chemoprotection in high-stage neuroblastoma. Oncogene 2020;39:1080–97.
37. Ribas A, Wolchok JD. Cancer immunotherapy using checkpoint blockade. Science 2018;359:1350–5.
38. Sharma A, Verhaagen J, Harvey AR. Receptor complexes for each of the class 3 semaphorins. Front Cell Neurosci 2012;6:28.
39. Greten FR, Grivennikov SI. Inflammation and cancer: triggers, mechanisms, and consequences. Immunity 2019;51:27–41.
40. Pascoe HG, Wang Y, Zhang X. Structural mechanisms of plexin signaling. Prog Biophys Mol Biol 2015;118:161–8.
41. Bustelo XR, Sauzeau V, Berenjeno IM. GTP-binding proteins of the Rho/Rac family: regulation, effectors, and functions in vivo. Bioessays 2007;29:356–70.
42. Roney KE, O'Connor BP, Wen H, Holl EK, Guthrie EH, Davis BK, et al. Plexin-B2 negatively regulates macrophage motility, Rac, and Cdc42 activation. PLoS One 2011;6:e24795.
43. Vikis HG, Li W, Guan KL. The plexin-B1/Rac interaction inhibits PAK activation and enhances Sema4D ligand binding. Genes Dev 2002;16:836–45.
44. Zhang N, Bevan MJ. $CD8^+$ T cells: foot soldiers of the immune system. Immunity 2011;35:161–8.
45. Suto F, Tsuboi M, Kamiya H, Mizuno H, Kiyama Y, Komai S, et al. Interactions between plexin-A2, plexin-A4, and semaphorin 6A control lamina-restricted projection of hippocampal mossy fibers. Neuron 2007;53:535–47.
46. Junqueira Alves C, Yotoko K, Zou H, Friedel RH. Origin and evolution of plexins, semaphorins, and Met receptor tyrosine kinases. Sci Rep 2019;9:1970.
47. Haklai-Topper L, Mlechkovich G, Savariego D, Gokhman I, Yaron A. Cis interaction between semaphorin 6A and plexin-A4 modulates the repulsive response to Sema6a. EMBO J 2010;29:2635–45.
48. Rozbesky D, Verhagen MG, Karia D, Nagy GN, Alvarez L, Robinson RA, et al. Structural basis of semaphorin–plexin cis interaction. EMBO J 2020;39: e102926.
49. Cagnoni G, Tamagnone L. Semaphorin receptors meet receptor tyrosine kinases on the way of tumor progression. Oncogene 2014;33:4795–802.
50. Melero I, Rouzaut A, Motz GT, Coukos G. T-cell and NK-cell infiltration into solid tumors: a key limiting factor for efficacious cancer immunotherapy. Cancer Discov 2014;4:522–6.
51. Mahoney KM, Rennert PD, Freeman GJ. Combination cancer immunotherapy and new immunomodulatory targets. Nat Rev Drug Discov 2015;14: 561–84.
52. Tumeh PC, Harview CL, Yearley JH, Shintaku IP, Taylor EJ, Robert L, et al. PD-1 blockade induces responses by inhibiting adaptive immune resistance. Nature 2014;515:568–71.
53. Brunner-Weinzierl MC, Rudd CE. CTLA-4 and PD-1 control of T-cell motility and migration: implications for tumor immunotherapy. Front Immunol 2018; 9:2737.
54. Wei SC, Duffy CR, Allison JP. Fundamental mechanisms of immune checkpoint blockade therapy. Cancer Discov 2018;8:1069–86.
55. Oestreich KJ, Yoon H, Ahmed R, Boss JM. NFATc1 regulates PD-1 expression upon T-cell activation. J Immunol 2008;181:4832–9.
56. Luo CT, Li MO. Foxo transcription factors in T-cell biology and tumor immunity. Semin Cancer Biol 2018;50:13–20.
57. Hedrick SM, Hess Michelini R, Doedens AL, Goldrath AW, Stone EL. FOXO transcription factors throughout T-cell biology. Nat Rev Immunol 2012;12: 649–61.
58. Valpione S, Galvani E, Tweedy J, Mundra PA, Banyard A, Middlehurst P, et al. Immune-awakening revealed by peripheral T-cell dynamics after one cycle of immunotherapy. Nat Cancer 2020;1:210–21.